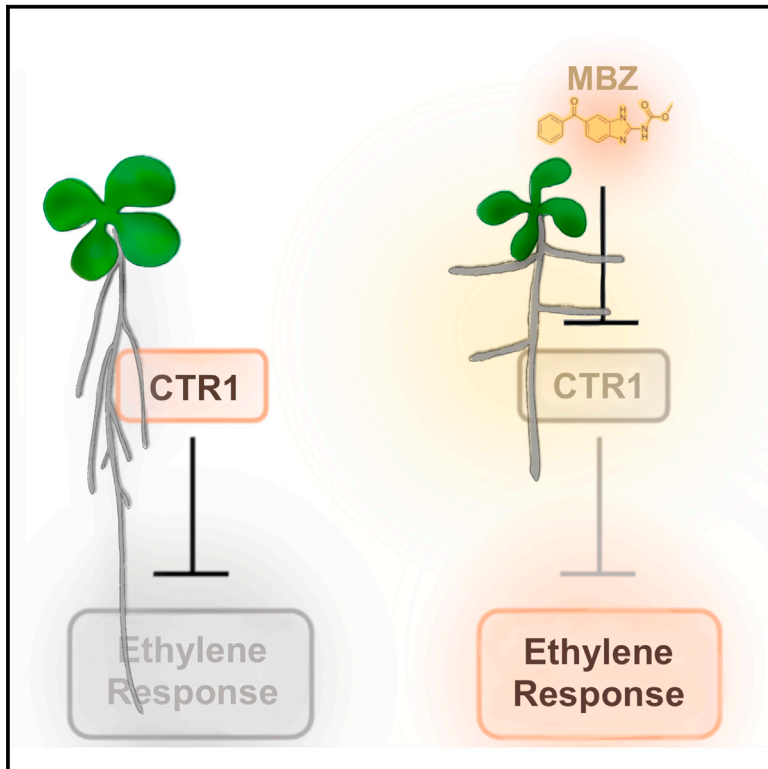


Identification of mebendazole as an ethylene signaling activator reveals a role of ethylene signaling in the regulation of lateral root angles

Graphical abstract



Authors

Wenrong He (何文容), Hai An Truong, Ling Zhang (张凌), ..., Kaizhen Zhong (钟开珍), Yingnan Hou (侯英楠), Wolfgang Busch

Correspondence

wbusch@salk.edu

In brief

He et al. identify a small molecule that regulates lateral root angle. They show that the compound increases lateral root angle by inhibiting CTR1 kinase activity, which in turn activates ethylene signaling. Therefore, they show that the ethylene pathway is involved in lateral root angle regulation.

Highlights

- MBZ increases lateral root angle
- MBZ regulates lateral root angle by activating ethylene signaling
- MBZ inhibits CTR1 kinase activity
- The ethylene pathway is involved in lateral root angle regulation



Article

Identification of mebendazole as an ethylene signaling activator reveals a role of ethylene signaling in the regulation of lateral root angles

Wenrong He (何文容),¹ Hai An Truong,¹ Ling Zhang (张凌),¹ Min Cao (曹珉),¹ Neal Arakawa,³ Yao Xiao (肖瑶),⁴ Kaizhen Zhong (钟开珍),¹ Yingnan Hou (侯英楠),^{5,6} and Wolfgang Busch^{1,2,7,*}

¹Plant Molecular and Cellular Biology Laboratory, Salk Institute for Biological Studies, La Jolla, CA 92037, USA

²Integrative Biology Laboratory, Salk Institute for Biological Studies, La Jolla, CA 92037, USA

³Environmental and Complex Analysis Laboratory (ECAL), Department of Chemistry and Biochemistry, University of California, San Diego, La Jolla, CA 92093, USA

⁴Department of Integrative Structural and Computational Biology, The Scripps Research Institute, La Jolla, CA 92037, USA

⁵Department of Microbiology and Plant Pathology, Center for Plant Cell Biology, University of California, Riverside, Riverside, CA 92521, USA

⁶School of Agriculture and Biology, Shanghai Jiao Tong University, Shanghai 200240, China

⁷Lead contact

*Correspondence: wbusch@salk.edu

<https://doi.org/10.1016/j.celrep.2024.113763>

SUMMARY

The lateral root angle or gravitropic set-point angle (GSA) is an important trait for root system architecture (RSA) that determines the radial expansion of the root system. The GSA therefore plays a crucial role for the ability of plants to access nutrients and water in the soil. Only a few regulatory pathways and mechanisms that determine GSA are known. These mostly relate to auxin and cytokinin pathways. Here, we report the identification of a small molecule, mebendazole (MBZ), that modulates GSA in *Arabidopsis thaliana* roots and acts via the activation of ethylene signaling. MBZ directly acts on the serine/threonine protein kinase CTR1, which is a negative regulator of ethylene signaling. Our study not only shows that the ethylene signaling pathway is essential for GSA regulation but also identifies a small molecular modulator of RSA that acts downstream of ethylene receptors and that directly activates ethylene signaling.

INTRODUCTION

The root systems of plants are vital for plant survival and productivity. They anchor plants and they absorb water and nutrients from the soil. The distribution of roots in the soil, root system architecture (RSA), is of enormous relevance. For instance, deeper rooting is associated with higher carbon permanence,¹ a critical trait for soil carbon sequestration and the ability of plants to survive terminal droughts.² Besides, to enhance the capacity for root systems to efficiently uptake nitrogen and water, deeper roots are required, yet for improving the uptake of phosphate and other nutrients, shallower soil layers have to be accessed by roots.³ A key determinant of RSA is the lateral root angle or gravitropic set-point angle (GSA). Previous studies have shown that auxin plays a crucial role in regulating GSA.^{4–6} Application of exogenous IAA or synthetic auxin leads to lateral root growth toward the vector of gravity thereby decreasing GSA.^{4,5} Another phytohormone, cytokinin, was also found to be involved in the regulation of GSA. Application of cytokinin showed an anti-gravitropic effect and thereby increased GSA.⁷ Finally, members of the IGT gene family, including DRO1/LAZY4, have been shown to play a major role in lateral root angles via auxin-associated mechanisms.^{8–11}

Ethylene is an ancient plant hormone. The ethylene signaling pathway is highly conserved and was present already in the aquatic progenitors of land plants.¹² Ethylene is produced from the conversion of S-adenosyl-L-methionine to 1-aminocyclopropane-1-carboxylic acid (ACC) and then to ethylene, which is catalyzed by enzymes including ACC synthase and ACC oxidase.^{13,14} When ethylene binds to its receptors (ETRs),^{15–17} it inactivates a serine/threonine protein kinase, CONSTITUTIVE TRIPLE RESPONSE1 (CTR1).¹⁸ In the absence of ethylene, CTR1 blocks ethylene downstream responses by phosphorylating the C-terminal end of ETHYLENE-INSENSITIVE2 (EIN2), an ER-associated membrane protein that works as a positive regulator of ethylene signaling.^{19–21} This leads to the degradation of EIN2-CEND by the Ub/26S proteasome.^{20–22} When CTR1 is inactivated by ethylene binding to ETRs, EIN2-CEND is stabilized and moves into the nucleus to transduce the ethylene signal to downstream transcription factors, such as EIN3, EIN3 LIKE1 (EIL1),^{23,24} and ETHYLENE RESPONSE FACTORS (ERFs).²⁵ These transcription factors activate the downstream ethylene response. The ethylene pathway was found to play an important role in numerous growth and developmental processes in the root, such as the inhibition of root elongation,^{18,26,27} induction of root hair growth,²⁸ and inhibition of the initiation of lateral roots.²⁹



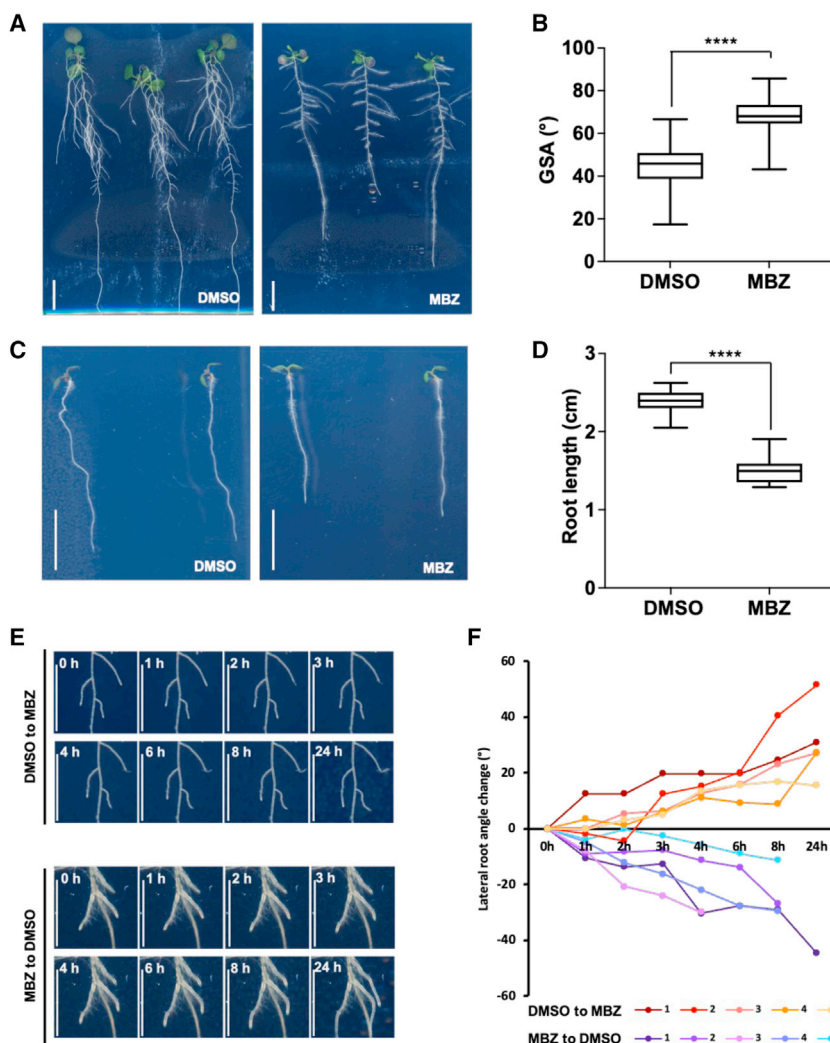


Figure 1. MBZ treatment perturbs root system architecture (RSA)

(A) 14-day-old Arabidopsis seedlings grown on DMSO and MBZ (1 μ M) plates.

(B) Quantification of GSA in (A). 15 lateral roots per seedling on DMSO plates, 12 lateral roots per seedling on MBZ plates, and 6 seedlings for each condition were used. Unpaired, two-tailed Student's *t* tests were used for statistical analysis. **** $p < 0.0001$.

(C) 7-day-old seedlings on DMSO and MBZ (1 μ M) plates.

(D) Quantification of primary root length (cm) in (B). 15–20 seedlings for each treatment were used. **** $p < 0.0001$.

(E) 14-day-old (upper panel) Arabidopsis seedlings on DMSO plates were transferred to MBZ (1 μ M) plates, and 19-day-old (bottom panel) seedlings on MBZ (1 μ M) plates were transferred to DMSO plates, followed by continuous scanning for 24 h. (F) Changes of lateral root angle after plate transfer from DMSO to MBZ (red and yellow lines) or MBZ to DMSO (blue, purple lines) compared to time point 0. (Scale bar: A and C, 1 cm; E, 5 mm). Boxplots: whiskers: min/max values; hinges: 25th to 75th percentile; mid-line: median. See also Figure S1.

To identify potential regulators of GSA, we performed a chemical genetics screen and identified a small molecule, mebendazole (MBZ), that dramatically increased GSA. Genetic analysis revealed that MBZ increased GSA through rapidly activating the ethylene signaling pathway. Both MBZ and ACC treatment induced ethylene signaling, which led to a modulation of lateral root angle. Further molecular and biochemistry studies showed that MBZ activates ethylene signaling by specifically targeting CTR1 and thereby blocking its kinase activity. Our study not only identified MBZ as an efficient small molecular activator of ethylene signaling, but it also uncovered that ethylene signaling plays an important role in regulating GSA.

RESULTS

A small compound profoundly affects the lateral root gravitropic set-point angle in Arabidopsis

To identify small molecules that affect GSA, we screened chemicals for their ability to change GSA of young seedlings from a small molecular library with 2,000 diverse generic chemicals

(SP 2000).^{30–32} We found that treatment with MBZ (Figure S1A) led to a distinct increase of lateral root angles that caused lateral roots to grow in a more horizontal direction (Figure 1A). The lateral root GSA of untreated 2-week-old Arabidopsis seedlings was approx. 46°, and the GSA of lateral roots of seedlings grown on 1- μ M MBZ plates was approx. 70° (Figures 1A and 1B). While the lateral root angle was the most striking phenotype, at a much earlier developmental stage (1 week after germination), seedlings on 1- μ M MBZ displayed a decreased root length (in average reduced by 37%) and an increased root hair initiation and elongation (Figures 1C, 1D, S1B, and S1C). To test how quickly MBZ would affect lateral root growth, we grew seedlings for 14 days on $\frac{1}{2}$ Murashige and Skoog (MS) medium with DMSO and then transferred them to $\frac{1}{2}$ MS medium supplemented with 1 μ M MBZ and acquired images every 10 min. All of the 5 measured lateral root tips started to grow at a more horizontal (less steep) angle within 3 h of MBZ treatment (Figures 1E, upper panel, and 1F), which coincided with the first time point at which root angles were significantly different between control and MBZ (Welch two sample *t* test; *p* value < 0.05). To test whether the action of MBZ was reversible, we germinated and grew seedlings on $\frac{1}{2}$ MS for 5 days and then transferred them to medium containing 1 μ M MBZ for 14 days, thereby inducing lateral roots of MBZ-treated seedlings to grow more horizontally. We note that we used this later time point (compared to the data presented in the upper panel) to be able to consider enough lateral roots that were growing at the more horizontal angle. We then transferred the seedlings back to control conditions and acquired images every

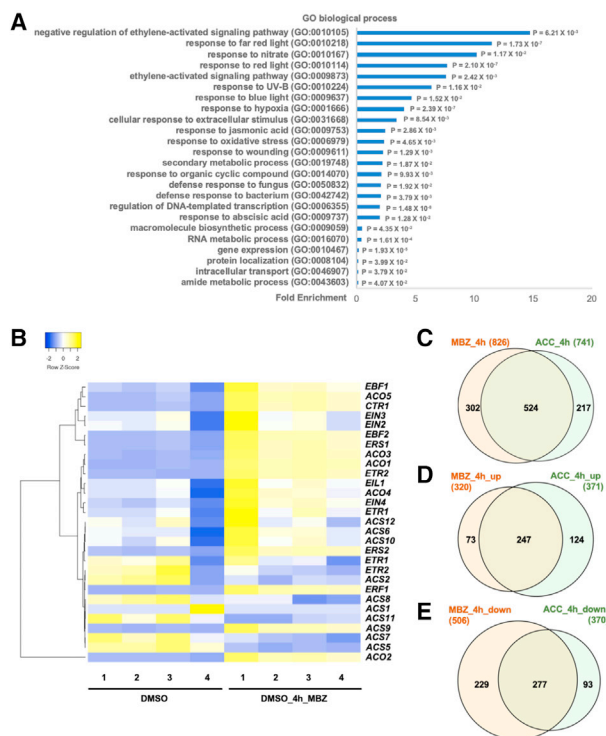


Figure 2. MBZ treatment regulates the ethylene pathway

(A) Gene Ontology (GO) analysis of upregulated genes (abs(log2) fold change > 1) from DEGs upon MBZ treatment in roots of 14-day-old Arabidopsis seedlings.

(B) Heatmap of DEGs involved in the ethylene pathway, which were detected to be differentially expressed upon MBZ treatment in the RNA-seq analysis. The left 4 columns of DMSO are data from 4 replicates of samples from DMSO (mock) plates. The right 4 columns of MBZ are data from 4 replicates of samples from MBZ treatment plates. The heatmap was made online by heatmapper (<http://heatmapper.ca/expression/>). The cluster method is complete linkage. Color bar indicates the relative expression level.

(C–E) Venn diagrams showing differentially expressed genes in 3-h MBZ treatment and 3-h ACC treatment. All genes (FDR < 0.05; abs(log2) fold change > 1) (C), upregulated genes (FDR < 0.05; log2 fold change > 1) (D), downregulated genes (log2 fold change < -1) (E).

(F) Dot plots showing the most enriched GO terms with KS p value < 0.05 from DEGs upon MBZ treatment in lateral root tips of 14-day-old seedlings.

(G–I) Representative images of lateral root tips of 2-week-old plants in response to negative control, positive control, and MBZ treatment using ethylene (*EIN3-GFP*) (G), auxin (*DR5v2-GFP*) (H), and cytokinin (*TCSn-GFP*) (I) reporter lines at 0 and 60 min of treatment.

(J) Relative fluorescent intensity of *EIN3-GFP* lateral root tips treated over a course of 4 h with DMSO, MBZ, and ACC.

(K) Relative fluorescent intensity of *DR5v2-GFP* lateral root tips treated over a course of 4 h with DMSO, MBZ, and IAA.

(L) Relative fluorescent intensity of *TCSn-GFP* lateral root tips treated over a course of 4 h with DMSO, MBZ, and tZ. 6 lateral roots for each treatment were used. Unpaired, two-tailed Student's t tests were used to compare the data of MBZ or the corresponding positive controls to DMSO at each time point. *p < 0.05; **p < 0.01; ***p < 0.001. See also Videos S1–S9.

10 min. Already after 1 h, root angles were significantly different between control (MBZ) and treatment (removal from MBZ) conditions (Welch two sample t test; p value < 0.05), and within 4 h, all 5 lateral root tips we measured started to grow at a distinctly steeper angle upon removal from MBZ (Figures 1E, bottom panel, and 1F). These data showed that the treatment of Arabidopsis roots with MBZ changes lateral root angles within 3 h and that this effect is fully reversible. In summary, we found that MBZ changes lateral root angles and important RSA traits associated with the development of a shallow root system.

Application of MBZ induces the ethylene pathway

To identify the pathway that MBZ acted upon, we utilized a genome-scale expression profiling approach. For this, we performed an mRNA-seq experiment using whole roots of 14-day-old Arabidopsis grown on ½ MS medium treated with 10 μM MBZ for 4 h. The analysis revealed that 677 genes were induced compared to mock treatment (false discovery rate [FDR] < 0.05; log2 fold change > 1), and 658 genes were repressed (FDR < 0.05; log2 fold change < -1). A Gene Ontology (GO) analysis revealed that among the genes that were upregulated by MBZ, genes involved in ethylene responses were strongly overrepresented in this early response. In particular, the GO process “negative regulation of ethylene-activated signaling pathway” (GO: 0010105) was the most enriched process (~21-fold enrichment, p value: 6.07×10^{-4}) upon MBZ treatment (Figure 2A), and the 4th most enriched GO process was “ethylene-activated signaling pathway” (GO: 0009873) (~11-fold enrichment, p value: 7.45×10^{-5}) (Figure 2A). Other GO categories were also significantly enriched, most notably

responses to light. However, given that ethylene signaling was the most enriched GO term, we first looked at the responses of genes involved in the ethylene hormone pathway. A major portion of these genes were differentially regulated by MBZ compared to mock treatment (Figures 2A and 2B). We therefore hypothesized that MBZ elicited the ethylene pathway. To test this hypothesis, we first compared the set of genes that had responded to MBZ with a published transcriptome dataset that had been generated by exposing roots to 4 h of ethylene treatment.³³ Of the 1,335 differentially expressed genes (DEGs) upon the 4 h of MBZ treatment, 306 were overlapping with 1,397 DEGs upon 4 h of ethylene treatment (p value for the overlap using a hypergeometric test: $p < 4.657 \times 10^{-143}$) (Figure S3A). Notably, more than 90% of these common DEGs retained the directionality of their expression change (i.e., genes upregulated by MBZ were also upregulated by ethylene treatment and vice versa) (Figures S3B and S3C). While this overlap was highly significant and supported the hypothesis that MBZ elicited ethylene responses, there was a high number of DEGs that didn't overlap. We reasoned that this might be due to differences in developmental and growth conditions of our MBZ-treated plants and of those plants used for the published ethylene treatment dataset.³³ For instance, we had used 14-day-old seedlings grown under long day conditions before we conducted the treatment, and the published data had utilized 3-day-old, dark-grown seedlings for eliciting the classical ethylene triple-response phenotype. To compare ethylene responses to MBZ responses under the same growth conditions and plant age, we performed another mRNA-seq experiment using roots of 14-day-old Arabidopsis grown on $\frac{1}{2}$ MS medium treated with 10 μ M MBZ or 10 μ M ACC (the ethylene precursor) for 3 h. We then again compared the overlap of the responsive genes. Out of 826 DEGs upon the MBZ treatment, 524 were overlapping with 741 DEGs upon 3 h of ACC treatment, accounting for 63% and 71% of DEGs upon MBZ and ACC treatment respectively (Figure 2C). 77% upregulated DEGs of the MBZ treatment overlapped with 65% upregulated DEGs of the ACC treatment (Figure 2D). These fractions were 54% and 75% for downregulated DEGs (Figure 2E). Taken together, our data strongly suggested that application of MBZ induces the ethylene pathway but in addition might also elicit non-ethylene-related effects.

MBZ induces ethylene responses

To investigate how MBZ treatment effects the ethylene response, we compared plant responses to MBZ and the ethylene precursor ACC. The most characteristic response to ethylene treatment is the triple response of etiolated seedlings³⁴ (Figures 3A–3C), which includes shortened and thickened roots and hypocotyls and an exaggerated apical hook. Consistent with our hypothesis that MBZ activates ethylene responses, 3-day-old etiolated seedlings treated with 10 μ M MBZ showed a prominent triple-response phenotype (Figures 3A–3C). Using different doses of MBZ, we found that 2.5 μ M of MBZ was sufficient to induce the triple-response phenotype in a dark environment (Figures S3A–S3F); we therefore started to use 2.5 μ M of MBZ to observe triple responses. Consistent with MBZ mimicking ethylene treatment, MBZ-induced triple response was abolished in the ethylene-insensitive mutants *ein2-5* and

ein3 eil1 (Figures S3D–S3F). Ethylene treatment inhibits root elongation mainly by repressing cell elongation rather than reducing the length of meristem.^{26,35} We therefore measured the length of root cells of 4-day-old etiolated seedlings treated with 2.5 μ M MBZ and 10 μ M ACC, and we found that similar to the ACC treatment, the mature cell size was reduced by MBZ treatment (Figures 3D–3F). Altogether, our data strongly suggested that MBZ elicits its effects via the ethylene pathway.

As we wanted to identify the mechanism by which MBZ changes the steepness of lateral root angles and given our data that MBZ acts on the ethylene pathway, we conducted an RNA-seq experiment on lateral root tips that had been treated either with DMSO or MBZ for 3 h. As sample collection was very challenging and took an hour per replicate, the sampled lateral roots had been treated for a time between 3 and 4 h. The most enriched GO categories were “regulation of transcription,” “response to auxin,” “ethylene activated signaling pathway,” and “cytokinin-signaling pathway” (Figure 2F). Given that the time window for the RNA-seq coincided with the change of lateral root angle, it was not surprising to detect auxin- and cytokinin-related genes, as these two hormonal pathways had been shown to be involved in determining the GSA of lateral roots.^{4,5,7} However, given the enrichment of genes assigned to these pathways, we wanted to check whether these pathways are activated before or after ethylene responses were elicited by MBZ. To do this, we obtained the *DR5-GFP V2* auxin response reporter line,³⁶ the *35S-EIN3-GFP* ethylene reporter line in the *ein3 eil1* background,³⁰ and the *TCN-GFP* cytokinin reporter line.³⁷ We then conducted time-lapse spinning disk confocal microscopy on lateral root tips from 14-day-old seedlings that were either treated with a DMSO control solution, MBZ, or the respective positive control (the auxin IAA, the cytokinin zeatin, or the ethylene precursor ACC). All positive control treatments swiftly induced the expression of the reporter genes in lateral roots (Figures 2G–2L; Videos S1, S3, S4, S6, S7, and S9). Consistent with our hypothesis that MBZ induced the ethylene pathway, MBZ treatment drastically induced the ethylene reporter within the first 20 min after treatment, even before the ethylene precursor ACC induced the reporter (Figures 2G and 2J; Videos S1, S2, and S3). MBZ treatment did not lead to an increased signal of the auxin response reporter, while the DMSO control led to a slight decrease of the reporter signal after 40 min, and the IAA treatment led to a strong increase throughout the whole duration of the experiment (Figures 2H and 2K; Videos S4, S5, and S6). There was no induction of the cytokinin reporter by MBZ in the time frame we observed the roots (Figures 2I and 2L; Videos S7, S8, and S9). Overall, these data strongly suggested that MBZ strongly and swiftly induces the ethylene pathway in lateral root tips.

MBZ activates ethylene signaling

Next, we set out to locate the target of MBZ in the ethylene pathway. First, we tested whether MBZ induces ethylene biosynthesis or acts on the perception of ethylene or on the ethylene signaling pathway. To test whether ethylene biosynthesis is affected, we measured ethylene production by GC-MS in 3-day-old etiolated Col-0 seedlings that were treated with 10 μ M MBZ or ACC. Ethylene production was dramatically

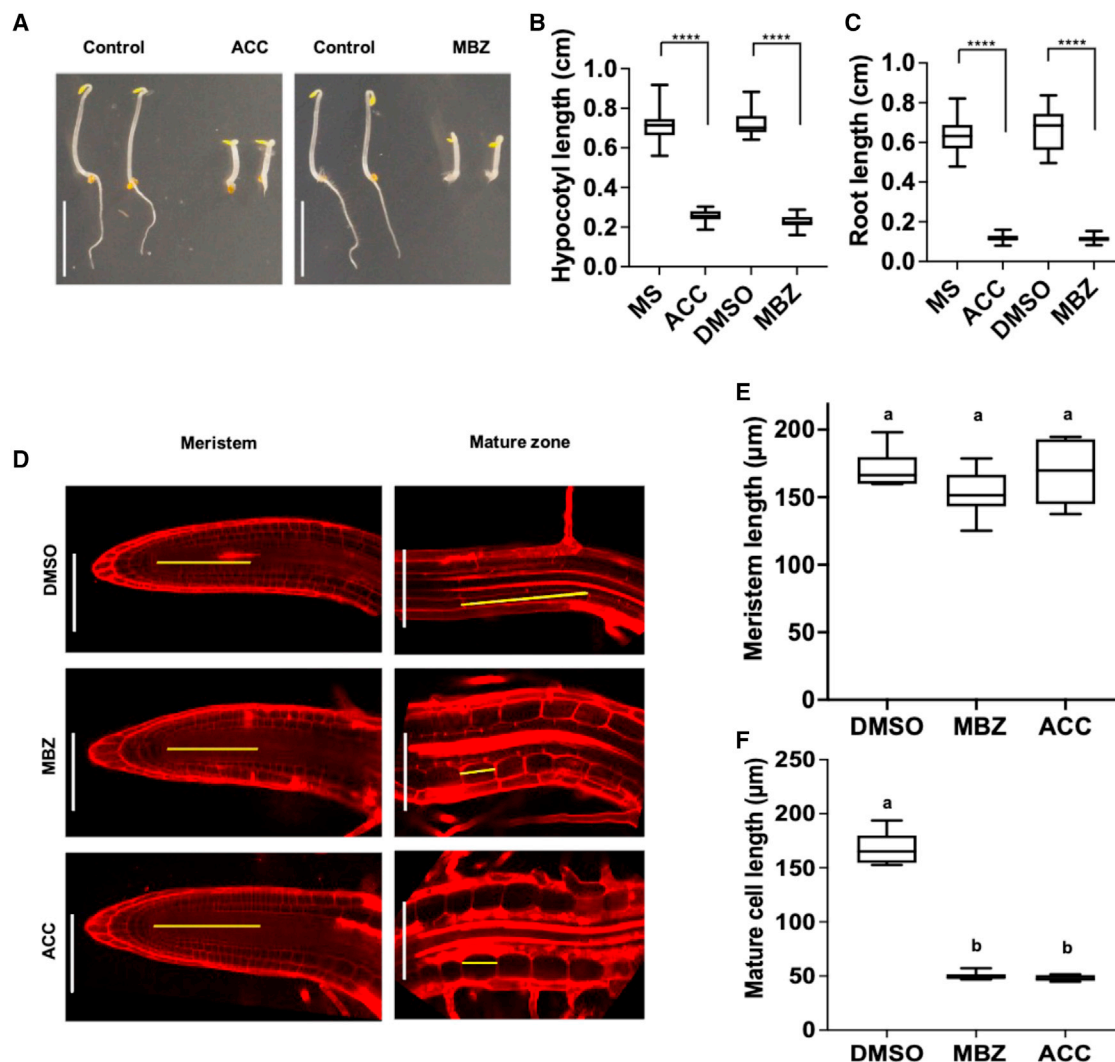


Figure 3. MBZ induces ethylene responses and mimics ACC treatment

(A) 4-day-old etiolated seedlings grown on MS, 10- μM ACC, DMSO, and 10- μM MBZ plates. 20 Col-0 seedlings for each treatment were observed, and 2 representative seedlings for each treatment are shown in the panel.

(B and C) Quantification of hypocotyl length (B) and primary root length (C) of seedlings in (A). 20 Col-0 seedlings for each treatment were used. **** $p < 0.0001$. (D) Images of median longitudinal optical sections of primary root meristem and mature zone stained with propidium iodide (PI) of 4-day-old etiolated Col-0 on DMSO, 2.5- μM MBZ, and 10- μM ACC plates; 6–10 seedlings were observed for each treatment.

(E and F) Meristem length (E) and mature cell size (F) of seedlings in (D). 6–10 seedlings for each treatment were used. Different letters label significant different values ($p < 0.0001$). One-way ANOVA and post hoc Tukey testing were used for statistical analysis in (E) and (F). (Scale bar: A, 5 mm; D, 100 μm). Boxplots: whiskers: min/max values; hinges: 25th to 75th percentile; mid-line: median.

induced by 10 μM ACC but not detected in DMSO or 10- μM MBZ-treated seedlings (Figure 4A). The results suggested that MBZ acts downstream of ethylene biosynthesis. To further test this hypothesis, we utilized gain-of-function mutants in the ethylene receptor *ETR1*. Root growth and GSA in strong *ETR1* alleles *etr1-1* and *etr1-3* were still strongly altered upon MBZ treatment (Figures 4B–4E). Moreover, 4-day-old etiolated seedlings of *etr1-3* treated with 2.5 μM MBZ showed the typical triple-response phenotype, demonstrating that ethylene responses are triggered by MBZ even without induced ethylene production or the perception of ethylene by *ETR1* (Figures S3A–S3C). In

contrast to the response to MBZ, *etr1-3* plants were completely insensitive to the treatment with 10 μM of ACC (Figures S3A–S3C). Collectively, these results show that MBZ induces ethylene responses by targeting factors downstream of ethylene biosynthesis and perception.

To uncover which components of ethylene signaling are targeted by MBZ, we studied MBZ responses in key mutants of the ethylene signaling pathway. First, we checked the root inhibition phenotype and GSA in *ctr1-1* mutant treated with MBZ and compared these responses to the Col-0 wild type. *CTR1* is the first negative regulator of ethylene signaling acting

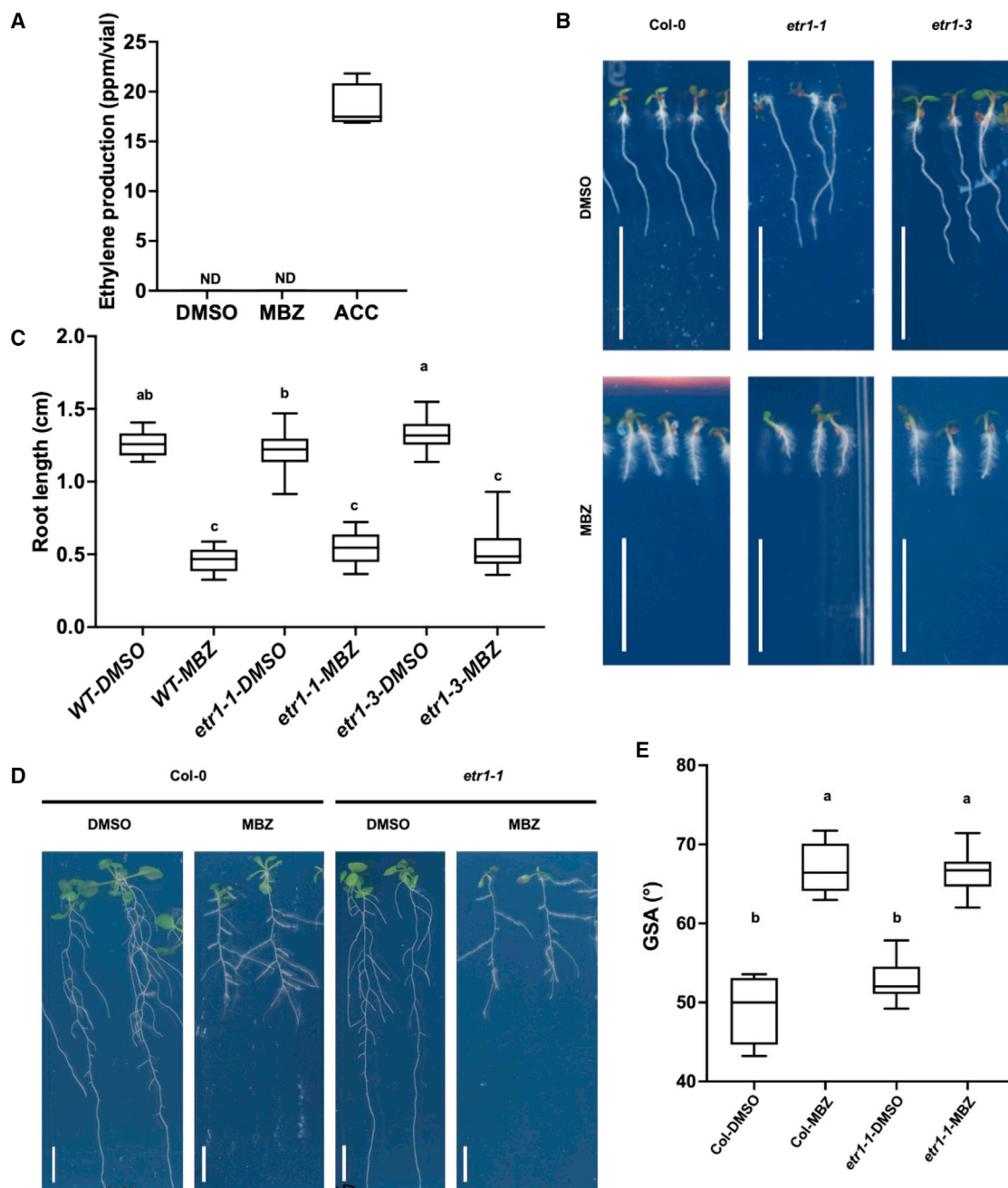


Figure 4. MBZ acts downstream of ethylene biosynthesis

(A) Quantification of ethylene production by GC-MS of 4-day-old etiolated seedlings of Col-0 in vials with DMSO, 10 μ M MBZ, and 10 μ M ACC medium. 100 seedlings for every vial and 4 biological replicates for each treatment; ND: not detectable.

(B) 6-day-old seedlings of Col-0, *etr1-1*, and *etr1-3* grown on DMSO and 1.2- μ M MBZ plates. 20 seedlings were observed.

(C) Quantification of root length in (A). 20 seedlings were quantified.

(D) 16-day-old seedlings of Col-0 and *etr1-1* grown on DMSO and 1.2- μ M MBZ plates. 20 seedlings were observed.

(E) Quantification of GSA in (C). 20 seedlings were quantified.

One-way ANOVA and post hoc Tukey testing were used for statistical analysis in (B) and (D). Different letters label significant different values ($p < 0.0001$). (Scale bar: B, D, 1 cm) Boxplots: whiskers: min/max values; hinges: 25th to 75th percentile; mid-line: median.

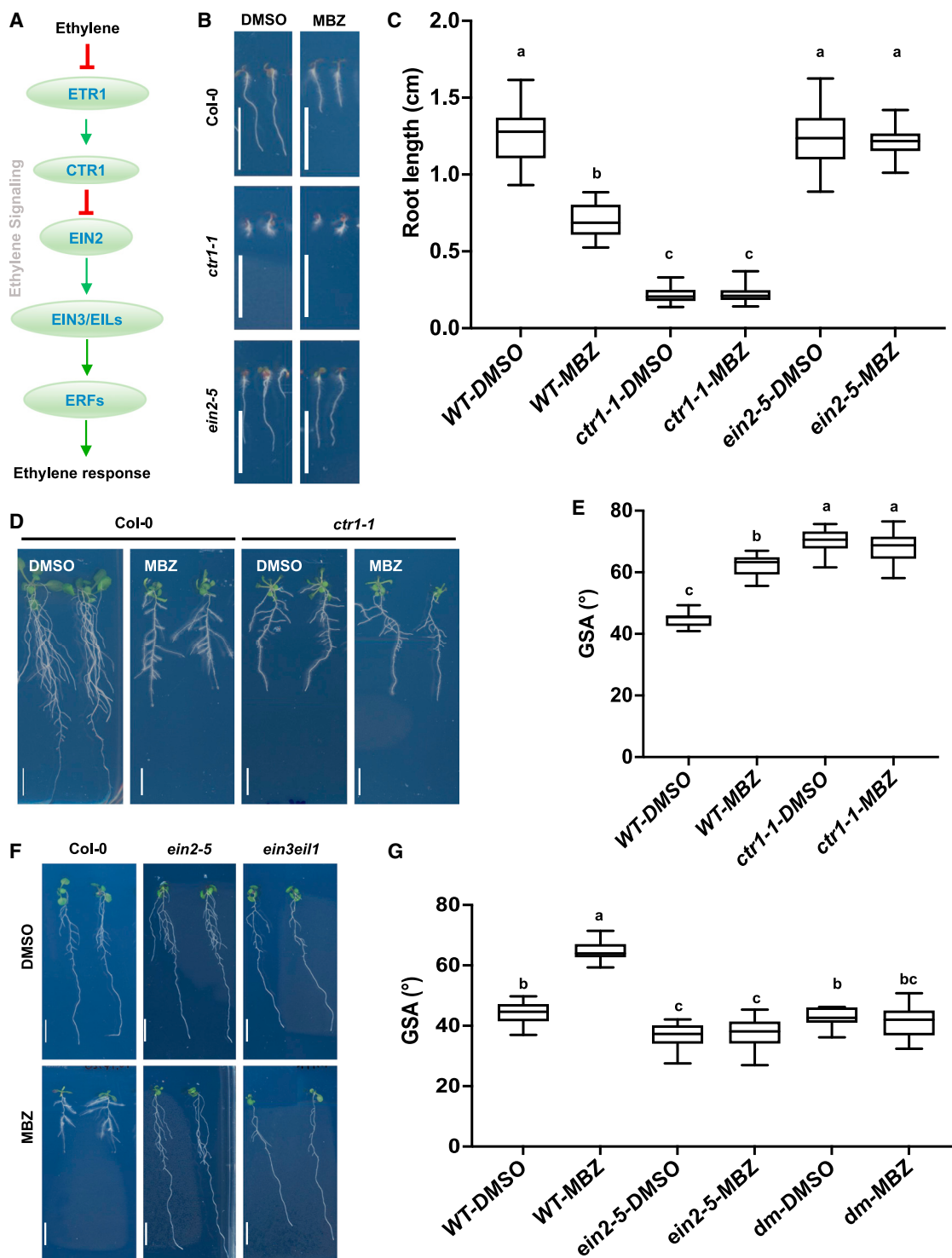


Figure 5. MBZ targets the ethylene signaling pathway

(A) Diagram of ethylene signaling pathway.

(B) 7-day-old seedlings of Col-0, *ctr1-1*, and *ein2-5* grown on DMSO and 1.2- μ M MBZ plates.

(C) Quantification of primary root length of seedlings in (B). 15–20 seedlings were quantified. Similar results were obtained from three biological replicates of the experiment.

(D) 19-day-old seedlings of Col-0 and *ctr1-1* grown on DMSO and 1.2- μ M MBZ plates.

(E) Quantification of GSA of seedlings in (D). 10 seedlings were quantified. Similar results were obtained from three biological replicates of the experiment.

(legend continued on next page)

downstream of ethylene receptors, and *EIN2* and *EIN3/EIL1* are positive regulators that act downstream of *CTR1* to trigger ethylene signaling (Figure 5A). Roots of Col-0 were sensitive to 1.2- μ M-MBZ treatment and showed short roots and increased root hair development (Figures 5B and 5C). However, *ctr1-1* mutants in which ethylene signaling is constitutively active showed short roots and abundant root hairs without any treatment at an early stage. Due to this pronounced early-seedling phenotype, we could not confidently assess changes in response to MBZ. However, we noticed that root growth remained insensitive to MBZ (Figures 5B and 5C). We further measured GSA at a later stage of development, which we had found to be a major effect of MBZ treatment. 3-week-old *ctr1-1* plants were insensitive to MBZ with regard to GSA (Figures 5D and 5E). Interestingly, *ctr1-1* without MBZ treatment showed an increased lateral root angle phenotype, which mimics MBZ treatment, suggesting that CTR1 might be the target of MBZ in ethylene signaling. Consistent with this hypothesis, root growth and GSA of *ein2-5* and *ein3 eil1* were clearly not affected by MBZ treatment (Figures 5B, 5C, 5F, and 5G), and in fact, *ein2-5* mutant plants, which are insensitive to ethylene, displayed steeper lateral root angles under control conditions compared to the wild type (Figures 5F and 5G). We further tested triple responses in *ctr1-1*, *ein2-5*, and *ein3 eil1* mutants. Consistent with the observation of root inhibition and GSA in *ctr1-1*, these plants showed a constitutive triple response regardless of MBZ treatment (Figures S3D–S3F). *ein2-5* and *ein3 eil1* plants were also insensitive to MBZ treatment (Figures S3D–S3F). Taken together, our data showed that MBZ activates ethylene signaling most likely by interfering with CTR1 in the ethylene signaling pathway.

MBZ is a potent inhibitor of CTR1 kinase activity

As MBZ hadn't induced the production of ethylene, and because MBZ had been able to elicit a typical triple response (the bona fide ethylene response) in *etr1* mutants, we focused on *CTR1*, which is the most upstream ethylene signaling gene that was insensitive to MBZ treatment. To pinpoint whether CTR1 is the target of MBZ, we capitalized on what is known about the activity of MBZ in mammalian systems. There, MBZ has been reported to be an inhibitor of the serine/threonine kinase *Homo sapiens* (*hs*) MAPK14.³⁸ Because CTR1 is also a serine/threonine protein kinase,¹⁸ we hypothesized that CTR1 is the direct target of MBZ in plants. Since it was shown that there are four critical amino acid residues in the catalytic site of *hs*MAPK14 that are relevant for MBZ binding,³⁸ we first tested *in silico* whether these residues were conserved between *hs*MAPK14 and CTR1. For this, we aligned the amino acid sequence of the Arabidopsis CTR1 and *hs*MAPK14 kinase domains (Figures 6A, S4A, and S4B). We found three (Lys 578, Thr 625, and Asp 694) of the four critical amino acid residues were conserved between the CTR1 kinase domain and that of *hs*MAPK14 (Figure 6A). The 4th critical residue is Met 109 in *hs*MAPK14, which corresponds to Leu 628 in CTR1. Because both Met and Leu are non-polar amino acids

with hydrophobic side chains and similar structure, it appeared possible that the replacement of Met by Leu in the CTR1 kinase domain does not significantly change the pocket structure for MBZ binding. We therefore hypothesized that the kinase domains of CTR1 and MAPK14 might have similar structures and function with regard to binding MBZ (Figure S4B).

To test this hypothesis, we first performed an *in silico* docking analysis using the published crystal structures of CTR1³⁹ (PDB: 3PPZ) and MBZ (ChEMBL: ChEMBL685). We found that MBZ is predicted to bind into the pocket of the CTR1 kinase domain (Figure 6B) formed by the aforementioned key amino acids (Figures 6A, 6B, and S4B). Overall, these analyses indicated that CTR1 could be the target of MBZ in Arabidopsis.

To further test this model, we expressed the recombinant kinase domains (KDs) of CTR1 and MAPK4 (a MAPK protein in Arabidopsis with a highly similar amino acid sequence to *hs*MAPK14) (Table S1; Figures S4C and S4D). We then confirmed the kinase inhibitory activity of MBZ through an *in vitro* phosphorylation assay via anti-thiophosphate-ester antibodies.⁴⁰ Using the phosphorylation state of myelin basic protein (MBP) (substrate) as the readout of the kinase activity, we found that MBZ inhibited the kinase activities of both CTR1-KD and MPK4 in a concentration-dependent manner; however, the inhibition for CTR1-KD was much more pronounced (Figures 6C and 6D). In particular, 10 μ M MBZ strongly inhibited the kinase activity of CTR1-KD, while 100 μ M MBZ totally blocked its activity. This assay demonstrated that MBZ can directly inhibit the kinase activity of CTR1-KD. Together with our genetic data that *ctr1-1* mutant mimicked the effect of MBZ on GSA and the triple-response phenotypes (Figures 5D, 5E, and S3D–S3F) and our molecular docking data (Figure 6B), our data strongly suggest that CTR1 is a direct target of MBZ in Arabidopsis. To further test the hypothesis that MBZ acts upon CTR1, we utilized a readout directly downstream of CTR1. Previous studies had shown that functional CTR1 phosphorylates the carboxyl end of EIN2, leading to its degradation.^{20–22} When ethylene inactivates CTR1, EIN2-CEND is stabilized and moves into the nucleus to activate downstream ethylene responses. We therefore tested if MBZ treatment mimicked ethylene for inducing EIN2 accumulation in the nucleus using 3-day-old etiolated seedlings of two independent transgenic *EIN2-GFP* reporter lines in which the GFP was fused to EIN2's C terminus (*pEIN2::EIN2-GFP* in the *ein2-5* background⁴¹). As expected, treatment with ACC quickly increased the nuclear accumulation of EIN2-GFP in root cells (Figures 7A, 7B, and S5). Consistent with our hypothesis that MBZ acted on CTR1, MBZ also significantly increased accumulation of EIN2-GFP in the nucleus (Figures 7A, 7B, and S5). Taken together, our data support a model in which MBZ is a small molecular inhibitor of the CTR1 kinase activity and thereby triggers the ethylene signaling pathway by permitting C-terminal EIN2 translocation into the nucleus, which in turn triggers ethylene downstream responses (Figures 7C and 7D).

(F) 16-day-old seedlings of Col-0 and *ein2-5* and *ein3 eil1* grown on DMSO and 1.2- μ M MBZ plates.

(G) Quantification of GSA of seedlings in (F). *dm* stands for *ein3 eil1* double mutants. One-way ANOVA and post hoc Tukey testing were used for statistical analysis in (C), (E), and (G). Different letters label significant different values ($p < 0.0001$). (Scale bar: B, D, F, 1 cm). Boxplots: whiskers: min/max values; hinges: 25th to 75th percentile; mid-line: median. See also Figure S3.

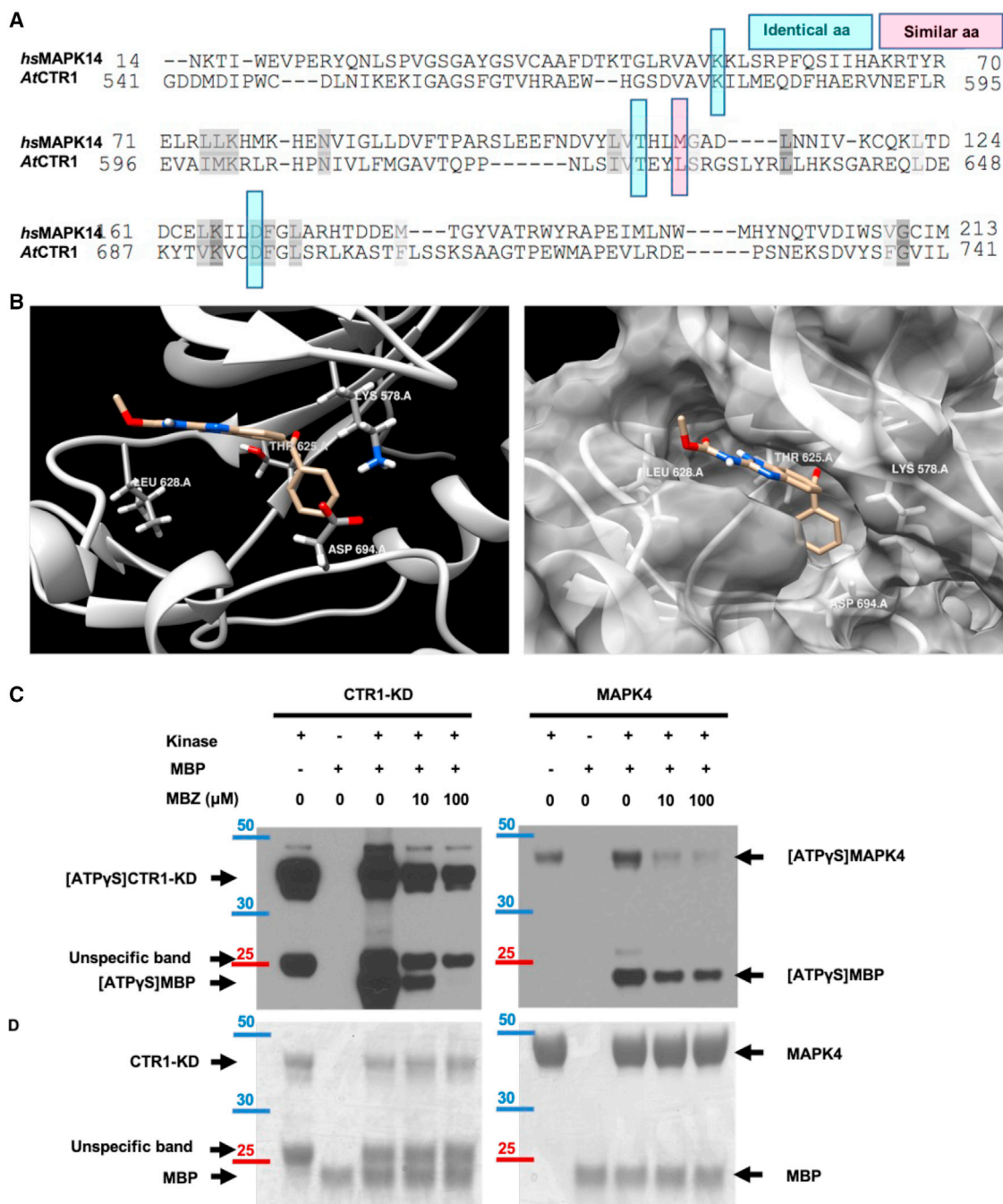


Figure 6. MBZ inhibits CTR1 kinase activity

(A) Sequence alignment of *hsMAPK14* and CTR1-KD in Arabidopsis around 4 core amino acids (highlighted by blue and pink frames) for MBZ binding.

(B) Molecular modeling of the interaction between MBZ (coppery) and CTR1-KD (silvery). In the left panel, the key residues that contribute to the binding with CTR1-KD were highlighted. The right panel showed the surface (gray) of the catalytic pocket of CTR1-KD.

(C) Western blot using recombinant anti-thiophosphate ester antibody under different concentration of MBZ treatment. Left panel: CTR1-KD; right panel: MAPK4. MBP is the substrate in both panels; MBZ concentrations are 0, 10, and 100 μM as labeled in different reactions; [ATPγS]CTR1-KD: ATPγS binding CTR1-KD, [ATPγS]MAPK4: ATPγS binding MAPK4, MBP that obtained ATPγS from CTR1-KD or MAPK4, which is labeled as [ATPγS]MBP. Note: ATPγS: adenosine 5'-(3-thiotriphosphate) tetralithium salt (Sigma, Cat# A1388).

(D) Coomassie blue staining of the gel shown in (C). CTR1: ~100 ng, MAPK4: ~1 μg. Myelin basic protein (MBP, a common kinase substrate, Sigma Cat. M1891): 2 μg, ATPγS: 1 mM. MBZ: 0, 10, or 100 μM. Arrows label the position of these bands on the gel. The molecular weight markers of the gels are labeled in blue and red color in (C) and (D). See also Figure S4.

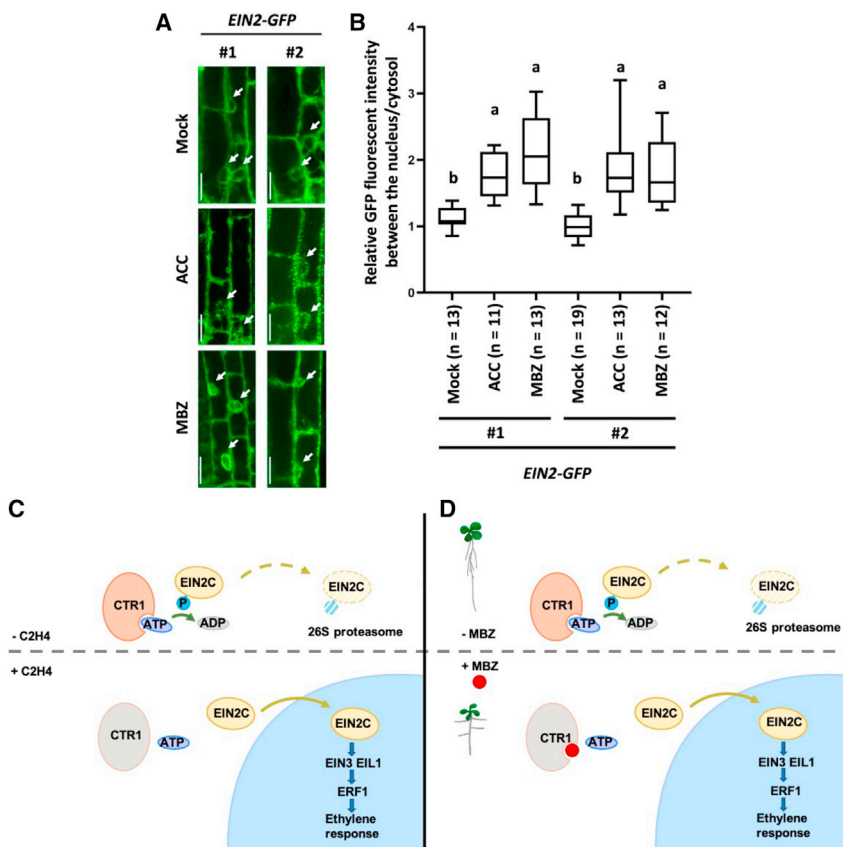


Figure 7. MBZ activates ethylene signaling

(A) Different patterns of nuclear accumulation of *EIN2-GFP* in root cells. 3-day-old etiolated seedlings treated with mock, ACC (100 μ M), or MBZ (10 μ M) for 3 h. Arrows indicate nuclei. Scale bar: 20 μ m.

(B) Quantification of relative GFP fluorescent intensity between the nucleus and cytosol of *EIN2-GFP* in (A). Boxplots: whiskers: min/max values; hinges: 25th to 75th percentile; mid-line: median. One-way ANOVA and post hoc Tukey testing were used for statistical analysis.

(C and D) Model for MBZ activation of ethylene signaling. (C) Ethylene suppresses CTR1 activity to promote *EIN2C* translocation and activates ethylene signaling. (D) MBZ inhibits CTR1 activity by binding to its kinase domain and promotes *EIN2C* translocation to activate the ethylene signaling. Note: *EIN2C*: C terminus of *EIN2*; ATP: adenosine triphosphate; ADP: adenosine diphosphate; C2H₄: ethylene; P: phosphate group. The CTR1 with orange color means active CTR1 proteins, and the CTR1 with gray color means inactive CTR1. See also Figure S5.

different tissues or conditions. While MBZ is not a perfect ethylene substitute and might have unspecific effects beyond activating ethylene signaling, as a direct activator of the ethylene signaling pathway, it promises to be a useful tool for the field. Such tools have been lacking so far

DISCUSSION

Our chemical genetic screen led to the identification of the small molecule MBZ that activates the ethylene signaling pathway. MBZ doesn't induce the production of ethylene (Figure 4A). The most upstream ethylene signaling gene insensitive to MBZ is *CTR1* (Figure 5), which encodes for a kinase whose phosphorylation activity is disrupted by MBZ (Figures 6C and 6D). Importantly, MBZ treatment elicited an important hallmark of ethylene signaling downstream of *CTR1*, which is the nuclear accumulation *EIN2* (Figures 7A, 7B, and S5). Taken together, these lines of evidence allowed us to pinpoint MBZ as an activator of ethylene signaling (Figure 7C). To our knowledge, MBZ is the first small molecule that acts downstream of ethylene receptors and that directly activates ethylene signaling. In previous studies, ethylene gas and ACC have been used to activate the ethylene signaling pathway. However, there were some disadvantages to using these approaches. In the case of treatment with ethylene gas, it is difficult to maintain a continuous treatment over longer periods of time due to the technical challenges for constantly maintaining the required ethylene concentrations. Because its controlled application is technically less challenging, ACC has been used more widely to study the role of ethylene. However, ACC was recently found to be a signaling molecule that can act independently of the ethylene pathway.⁴² Moreover, the necessity for enzymatic ACC conversion to ethylene in plants might be limiting in

despite several attempts that have been made to identify small molecular regulators of ethylene signaling. Neither approaches targeting ethylene biogenesis and perception nor approaches targeting downstream auxin biosynthesis had yielded in molecules acting on ethylene signaling.^{30–32,43}

Because *CTR1* contains the critical MBZ binding residues that had been elucidated in the human MBZ target *hsMPK14*, and because of the profound genetic evidence for *CTR1*, it is somewhat unlikely that other components in the ethylene pathway such as the E3 ligases *ETP1/2* and *EBF1/2*, which negatively regulate *EIN2* and *EIN3* respectively,^{44,45} are targets of MBZ. Another signaling pathway that impinges on ethylene signaling is the glucose-activated TOR signaling pathway, which had recently been shown to regulate *EIN2* activity through phosphorylation.⁴¹ However, the TOR kinase does not contain any of the 4 key residues known for MBZ binding. Moreover, unlike MBZ, none of the inhibitors of TOR, including Rap, Torin2, and AMA, did induce the ethylene-induced triple-response phenotype.⁴⁶ In addition, *ein2-5* and *ein3 eil1* mutants displayed a shorter hypocotyl when the Glu-TOR-*EIN2* pathway was inhibited⁴⁶ (Figure 1B), but these mutants did not respond to MBZ treatment (Figures S3D and S3E). Altogether, it is most likely that the observed response of MBZ on the ethylene signaling is exerted via its binding to *CTR1*.

While most of the effects of MBZ are related to its activation of ethylene signaling, our RNA profiling indicated additional effects of MBZ. Consistently, treatment with a high concentration of

MBZ or long-term treatment with it led to strongly inhibited plant growth and development, including a disrupted root apical meristem and morphological changes of leaves. These phenotypes have not been observed upon ethylene treatment (Figures S6A and S6B), raising the possibility that MBZ may have other targets in plants. MAPK4 has the highest amino acid sequence similarity to the human MBZ target *hsMAPK14* (Table S1). Compared to CTR1, the effect of MBZ on MAPK4 kinase activity was much less pronounced (Figure 6C), consistent with the lack of conservation of key amino acids relevant for MBZ binding (Figure S4C). Although MBZ couldn't inhibit the kinase activity of MAPK4 as strongly as that of CTR1-KD, a decrease of the weak MAPK4 autophosphorylation band might indicate that MBZ treatment can disrupt MAPK4 autophosphorylation (Figure 6C). This raises the possibility that MBZ might alter autophosphorylation of MAPK4 and probably other CTR1-like kinases, based on the sequence conservation of the four critical residues (Figures 6A and S4B). This might explain the additional effects of MBZ. Additionally, there are a number of CTR1 paralogs in Arabidopsis. These include the kinases encoded by AT4G24480, AT1G08720, At1g18160, AT1G67920, and AT5G11850. These kinases contain all four critical amino acids, raising the possibility that MBZ may also bind to these paralogs. Another explanation for the observed effects of MBZ that go beyond observed ethylene effects might be that continuous activation of ethylene signaling via CTR1 might have more complicated or compounded effects than are elicited by external ethylene or ACC treatment (Figure S6C). Support for this comes from the *ctr1-1* mutant, which is dwarfed and shows aberration in leaf shape and thereby displays much stronger phenotypes than elicited with ACC or ethylene treatment¹⁸ (Figures 5B–5D and S6C). While MBZ's predominant effect on ethylene signaling via CTR1 is strongly supported by our study, further studies will be needed to elucidate the details of MBZ specificity.

One of the most intriguing effects of MBZ on the plant is its potent ability to change GSA. This suggests that ethylene signaling is involved in the regulation of the GSA in lateral roots. While important regulatory roles for GSA are known for auxin and cytokinin, and there can be complex interplays between auxin, cytokinin, and ethylene, the induction of the ethylene signaling pathway clearly dominated responses in lateral roots after they were treated with MBZ (Figure 2). This activation of the ethylene responses occurred before angles of lateral roots were changing and was maintained throughout the timescale at which GSA was changed by the MBZ treatment, which occurred after 1–4 h of MBZ treatment (Figures 1E, 1F, 2, and S2I). In our study, we found that MBZ didn't induce ethylene biosynthesis (Figure 4A). ACC treatment had a weak but distinct effect on root angle and displayed concentration-dependent effects when applying a large range of concentrations (Figure S6C). Strong direct evidence for the impact of ethylene signaling in regulating lateral root set-point angle is provided by the RSA phenotype of the *ctr1-1* mutant. In *ctr1-1*, ethylene signaling is constitutively activated and leads to an increased lateral root angle (Figures 5D and 5E). Conversely, we observed that the ethylene-insensitive *ein2-5* mutant displays steeper lateral roots (Figures 5F and 5G). Overall, this exposes a yet unknown role of ethylene signaling in the regulation of lateral root set-point angle. One

reason why the role of ethylene in the regulation of lateral root angles hasn't been recognized so far might be that it reduces lateral root formation by itself,²⁹ making the study of lateral root angles more difficult. Our study strongly suggests that it will be worthwhile to explore the role of ethylene and its interaction with auxin and cytokinin in root gravitropism and RSA. Moreover, MBZ might also be used as a versatile tool for exploring the molecular mechanisms of root gravitropism and lateral root set-point angles since as a small molecule, and due to its reversible mode of action, it can be easily applied to elicit controlled changes of lateral root angles. It might also be useful to reveal the mechanisms underlying GSA regulation by phytohormones and known GSA signals, such as the *LAZY* family genes.⁴⁷ Finally, since ethylene signaling is a widely conserved process in land plants, exploring the ability of MBZ or genetic perturbation of the ethylene pathway to change RSA in crop species might be highly worthwhile for RSA engineering.

Limitations of the study

While we have shown that MBZ predominantly acts on the ethylene pathway, it is possible that MBZ has effects that are independent of the ethylene pathway. In this study we didn't explore MBZ effects that are not related to the ethylene pathway, other than showing that it might have a minor effect on the MAPK4 kinase activity (which has the highest amino acid sequence similarity to the human MBZ target *hsMAPK14*). Being a kinase inhibitor, MBZ might also affect other kinases. Therefore, measuring the effects of MBZ on the phosphorylation activity of other kinases could have shed more light on potential ethylene-signaling-independent aspects.

We investigated the effect of MBZ and ethylene signaling on lateral root angles in seedlings grown on agar plates in our standard growth conditions. We didn't explore to which extent these effects will be relevant in other environments such as in soil or in seedlings grown under other temperature or light conditions. Like for any other study that was performed in specific environments, it will be important to assess whether the observed effects on lateral root angle will be affected by environmental parameters.

STAR★METHODS

Detailed methods are provided in the online version of this paper and include the following:

- KEY RESOURCES TABLE
- RESOURCE AVAILABILITY
 - Lead contact
 - Materials availability
 - Data and code availability
- EXPERIMENTAL MODEL AND SUBJECT DETAILS
 - *Arabidopsis thaliana*
 - Accession numbers
- METHOD DETAILS
 - Small molecule library and screen information
 - Cloning and constructs
 - Chemical solutions
 - Root phenotyping

- Lateral root angle measurement
- Time lapse of lateral root angle phenotyping
- mRNA-seq
- B. data analysis
- GO analysis
- Measurement of ethylene production
- Microscopy
- Accumulation of EIN2-GFP in root cells
- Time lapse microscopy of reporter genes in lateral root tips
- Quantification of relative GFP fluorescent intensity between the nucleus and cytosol
- Computational docking and molecular modeling
- Protein purification
- *In vitro* kinase assay with non-radioactive ATP- γ -S
- **QUANTIFICATION AND STATISTICAL ANALYSIS**

SUPPLEMENTAL INFORMATION

Supplemental information can be found online at <https://doi.org/10.1016/j.celrep.2024.113763>.

ACKNOWLEDGMENTS

The research was supported by start-up funds from the Salk Institute for Biological Studies and funds from the Harnessing Plants Initiative to W.B. and a Salk Women & Science Special Award and a Pioneer Fund Postdoctoral Scholar Award to W.H. We are grateful to Dr. Glenn R. Hicks and Dr. Natasha Raikhel for sharing the SP2000 small molecule library. We thank Dr. Cris Argueso, Dr. Dolf Weijers, and Dr. Liwen Fu for sharing seeds. We also thank Dr. Joseph R. Ecker and Dr. Joanne Chory for critical discussions. We thank the Next Generation Sequencing Core of Salk Institute for NGS Library preparation and sequencing. This work was supported by the NGS Core Facility of the Salk Institute with funding from NIH-NCI CCSG: P30 CA01495, NIH-NIA San Diego Nathan Shock Center P30 AG068635, and the Chapman Foundation and the Helmsley Charitable Trust. We also thank Matthieu Platré, Nicole Gibbs, Anna Malolepszy, Björn Willige, Travis Lee, and Liwen Fu for fruitful discussions and suggestions.

AUTHOR CONTRIBUTIONS

W.H. and W.B. conceived the project and the experiments. W.H. performed the SP2000 library screen and analysis with help from Y.H. W.H. performed the phenotyping, alignment, docking, protein purification, and kinase activity assay. W.H. conducted the microscopy and mRNA-seq on primary roots with help from K.Z. H.A.T. performed the time lapse reporter analysis using spinning disk microscopy, as well as the whole root system and lateral root RNA-seq experiments. L.Z. conducted the mRNA-seq analysis and the statistical analysis. W.H. conducted heatmap analysis of mRNA-seq. W.H. and L.Z. conducted Gene Ontology analysis. M.C. provided the protocol and suggestions for kinase activity assay. N.A. performed the GC test. Y.X. performed the FPLC. W.H. and W.B. wrote the manuscript with input from all authors. W.B. provided materials, funding, supervision, guidance, and advice on the project, the experiments, and the analysis of the results.

DECLARATION OF INTERESTS

W.B. is a co-founder of Cquesta, a company that works on crop root growth and carbon sequestration.

Received: April 23, 2022

Revised: August 31, 2023

Accepted: January 24, 2024

Published: February 13, 2024

REFERENCES

1. Poirier, V., Roumet, C., and Munson, A.D. (2018). The root of the matter: Linking root traits and soil organic matter stabilization processes. *Soil Biol. Biochem.* 120, 246–259. <https://doi.org/10.1016/j.soilbio.2018.02.016>.
2. Uga, Y., Sugimoto, K., Ogawa, S., Rane, J., Ishitani, M., Hara, N., Kitomi, Y., Inukai, Y., Ono, K., Kanno, N., et al. (2013). Control of root system architecture by DEEPER ROOTING 1 increases rice yield under drought conditions. *Nat. Genet.* 45, 1097–1102. <https://doi.org/10.1038/ng.2725>.
3. Lynch, J.P. (2019). Root phenotypes for improved nutrient capture: an underexploited opportunity for global agriculture. *New Phytol.* 223, 548–564. <https://doi.org/10.1111/nph.15738>.
4. Roychoudhry, S., Del Bianco, M., Kieffer, M., and Kepinski, S. (2013). Auxin controls gravitropic setpoint angle in higher plant lateral branches. *Curr. Biol.* 23, 1497–1504. <https://doi.org/10.1016/j.cub.2013.06.034>.
5. Rosquete, M.R., von Wangenheim, D., Marhavý, P., Barbez, E., Stelzer, E.H.K., Benková, E., Maizel, A., and Kleine-Vehn, J. (2013). An auxin transport mechanism restricts positive orthogravitropism in lateral roots. *Curr. Biol.* 23, 817–822. <https://doi.org/10.1016/j.cub.2013.03.064>.
6. Xiao, G., and Zhang, Y. (2020). Adaptive Growth: Shaping Auxin-Mediated Root System Architecture. *Trends Plant Sci.* 25, 121–123. <https://doi.org/10.1016/j.tplants.2019.12.001>.
7. Waidmann, S., Ruiz Rosquete, M., Schöller, M., Sarkel, E., Lindner, H., LaRue, T., Petrik, I., Dünser, K., Martopawiro, S., Sasidharan, R., et al. (2019). Cytokinin functions as an asymmetric and anti-gravitropic signal in lateral roots. *Nat. Commun.* 10, 3540. <https://doi.org/10.1038/s41467-019-11483-4>.
8. Ge, L., and Chen, R. (2016). Negative gravitropism in plant roots. *Nat. Plants* 2, 16155. <https://doi.org/10.1038/nplants.2016.155>.
9. Guseman, J.M., Webb, K., Srinivasan, C., and Dardick, C. (2017). DRO1 influences root system architecture in Arabidopsis and Prunus species. *Plant J.* 89, 1093–1105. <https://doi.org/10.1111/tpj.13470>.
10. Yoshihara, T., and Spalding, E.P. (2017). LAZY Genes Mediate the Effects of Gravity on Auxin Gradients and Plant Architecture. *Plant Physiology* (Bethesda) 175, 959–969. <https://doi.org/10.1104/pp.17.00942>.
11. Waite, J.M., and Dardick, C. (2021). The roles of the IGT gene family in plant architecture: past, present, and future. *Curr. Opin. Plant Biol.* 59, 101983. <https://doi.org/10.1016/j.cop.2020.101983>.
12. Ju, C., Van de Poel, B., Cooper, E.D., Thierer, J.H., Gibbons, T.R., Delwiche, C.F., and Chang, C. (2015). Conservation of ethylene as a plant hormone over 450 million years of evolution. *Nat. Plants* 1, 14004. <https://doi.org/10.1038/nplants.2014.4>.
13. Yang, S.F., and Hoffman, N.E. (1984). Ethylene Biosynthesis and its Regulation in Higher Plants. *Annu. Rev. Plant Physiol.* 35, 155–189. <https://doi.org/10.1146/annurev.pp.35.060184.001103>.
14. Pattyn, J., Vaughan-Hirsch, J., and Van de Poel, B. (2021). The regulation of ethylene biosynthesis: a complex multilevel control circuitry. *New Phytol.* 229, 770–782. <https://doi.org/10.1111/nph.16873>.
15. Chang, C., Kwok, S.F., Bleecker, A.B., and Meyerowitz, E.M. (1993). Arabidopsis ethylene-response gene ETR1: similarity of product to two-component regulators. *Science* 262, 539–544. <https://doi.org/10.1126/science.8211181>.
16. Sakai, H., Hua, J., Chen, Q.G., Chang, C., Medrano, L.J., Bleecker, A.B., and Meyerowitz, E.M. (1998). ETR2 is an ETR1-like gene involved in ethylene signaling in Arabidopsis. *Proc. Natl. Acad. Sci. USA* 95, 5812–5817. <https://doi.org/10.1073/pnas.95.10.5812>.
17. Hua, J., Sakai, H., Nourizadeh, S., Chen, Q.G., Bleecker, A.B., Ecker, J.R., and Meyerowitz, E.M. (1998). EIN4 and ERS2 are members of the putative ethylene receptor gene family in Arabidopsis. *Plant Cell* 10, 1321–1332. <https://doi.org/10.1105/tpc.10.8.1321>.
18. Kieber, J.J., Rothenberg, M., Roman, G., Feldmann, K.A., and Ecker, J.R. (1993). CTR1, a negative regulator of the ethylene response pathway in

- Arabidopsis, encodes a member of the raf family of protein kinases. *Cell* 72, 427–441. [https://doi.org/10.1016/0092-8674\(93\)90119-b](https://doi.org/10.1016/0092-8674(93)90119-b).
19. Alonso, J.M., Hirayama, T., Roman, G., Nourizadeh, S., and Ecker, J.R. (1999). EIN2, a bifunctional transducer of ethylene and stress responses in Arabidopsis. *Science* 284, 2148–2152. <https://doi.org/10.1126/science.284.5423.2148>.
20. Ju, C., Yoon, G.M., Shemansky, J.M., Lin, D.Y., Ying, Z.L., Chang, J., Garrett, W.M., Kessenbrock, M., Groth, G., Tucker, M.L., et al. (2012). CTR1 phosphorylates the central regulator EIN2 to control ethylene hormone signaling from the ER membrane to the nucleus in Arabidopsis. *Proc. Natl. Acad. Sci. USA* 109, 19486–19491. <https://doi.org/10.1073/pnas.1214848109>.
21. Wen, X., Zhang, C., Ji, Y., Zhao, Q., He, W., An, F., Jiang, L., and Guo, H. (2012). Activation of ethylene signaling is mediated by nuclear translocation of the cleaved EIN2 carboxyl terminus. *Cell Res.* 22, 1613–1616. <https://doi.org/10.1038/cr.2012.145>.
22. Qiao, H., Shen, Z., Huang, S.S.C., Schmitz, R.J., Urlich, M.A., Briggs, S.P., and Ecker, J.R. (2012). Processing and subcellular trafficking of ER-tethered EIN2 control response to ethylene gas. *Science* 338, 390–393. <https://doi.org/10.1126/science.1225974>.
23. Chao, Q., Rothenberg, M., Solano, R., Roman, G., Terzaghi, W., and Ecker, J.R. (1997). Activation of the ethylene gas response pathway in Arabidopsis by the nuclear protein ETHYLENE-INSENSITIVE3 and related proteins. *Cell* 89, 1133–1144. [https://doi.org/10.1016/S0092-8674\(00\)80300-1](https://doi.org/10.1016/S0092-8674(00)80300-1).
24. An, F., Zhao, Q., Ji, Y., Li, W., Jiang, Z., Yu, X., Zhang, C., Han, Y., He, W., Liu, Y., et al. (2010). Ethylene-induced stabilization of ETHYLENE INSENSITIVE3 and EIN3-LIKE1 is mediated by proteasomal degradation of EIN3 binding F-box 1 and 2 that requires EIN2 in Arabidopsis. *Plant Cell* 22, 2384–2401. <https://doi.org/10.1105/tpc.110.076588>.
25. Müller, M., and Munné-Bosch, S. (2015). Ethylene Response Factors: A Key Regulatory Hub in Hormone and Stress Signaling. *Plant Physiol.* 169, 32–41. <https://doi.org/10.1104/pp.15.00677>.
26. Vaseva, I.I., Qudeimat, E., Potuschak, T., Du, Y., Genschik, P., Vandenbussche, F., and Van Der Straeten, D. (2018). The plant hormone ethylene restricts Arabidopsis growth via the epidermis. *Proc. Natl. Acad. Sci. USA* 115, E4130–E4139. <https://doi.org/10.1073/pnas.1717649115>.
27. Le, J., Vandenbussche, F., Van Der Straeten, D., and Verbelen, J.P. (2001). In the early response of Arabidopsis roots to ethylene, cell elongation is up- and down-regulated and uncoupled from differentiation. *Plant Physiol.* 125, 519–522. <https://doi.org/10.1104/pp.125.2.519>.
28. Feng, Y., Xu, P., Li, B., Li, P., Wen, X., An, F., Gong, Y., Xin, Y., Zhu, Z., Wang, Y., and Guo, H. (2017). Ethylene promotes root hair growth through coordinated EIN3/EIL1 and RHD6/RSL1 activity in Arabidopsis. *Proc. Natl. Acad. Sci. USA* 114, 13834–13839. <https://doi.org/10.1073/pnas.1711723115>.
29. Negi, S., Ivanchenko, M.G., and Muday, G.K. (2008). Ethylene regulates lateral root formation and auxin transport in Arabidopsis thaliana. *Plant J.* 55, 175–187. <https://doi.org/10.1111/j.1365-3113X.2008.03495.x>.
30. He, W., Brumos, J., Li, H., Ji, Y., Ke, M., Gong, X., Zeng, Q., Li, W., Zhang, X., An, F., et al. (2011). A Small-Molecule Screen Identifies L-Kynurenine as a Competitive Inhibitor of TAA1/TAR Activity in Ethylene-Directed Auxin Biosynthesis and Root Growth in Arabidopsis. *Plant Cell* 23, 3944–3960. <https://doi.org/10.1105/tpc.111.089029>.
31. Sun, X., Li, Y., He, W., Ji, C., Xia, P., Wang, Y., Du, S., Li, H., Raikhel, N., Xiao, J., and Guo, H. (2017). Pyrazinamide and derivatives block ethylene biosynthesis by inhibiting ACC oxidase. *Nat. Commun.* 8, 15758. <https://doi.org/10.1038/ncomms15758>.
32. Zhu, Y., Li, H.J., Su, Q., Wen, J., Wang, Y., Song, W., Xie, Y., He, W., Yang, Z., Jiang, K., and Guo, H. (2019). A phenotype-directed chemical screen identifies ponalrestat as an inhibitor of the plant flavin monooxygenase YUCCA in auxin biosynthesis. *J. Biol. Chem.* 294, 19923–19933. <https://doi.org/10.1074/jbc.RA119.010480>.
33. Chang, K.N., Zhong, S., Weirauch, M.T., Hon, G., Pelizzola, M., Li, H., Huang, S.S.C., Schmitz, R.J., Urlich, M.A., Kuo, D., et al. (2013). Temporal transcriptional response to ethylene gas drives growth hormone cross-regulation in Arabidopsis. *Elife* 2, e00675. <https://doi.org/10.7554/eLife.00675>.
34. Guzmán, P., and Ecker, J.R. (1990). Exploiting the triple response of Arabidopsis to identify ethylene-related mutants. *Plant Cell* 2, 513–523. <https://doi.org/10.1105/tpc.2.6.513>.
35. De Cnodder, T., Vissenberg, K., Van Der Straeten, D., and Verbelen, J.P. (2005). Regulation of cell length in the Arabidopsis thaliana root by the ethylene precursor 1-aminocyclopropane-1-carboxylic acid: a matter of apoptotic reactions. *New Phytol.* 168, 541–550. <https://doi.org/10.1111/j.1469-8137.2005.01540.x>.
36. Liao, C.Y., Smet, W., Brunoud, G., Yoshida, S., Vernoux, T., and Weijers, D. (2015). Reporters for sensitive and quantitative measurement of auxin response. *Nat. Methods* 12, 207–210. <https://doi.org/10.1038/nmeth.3279>.
37. Zürcher, E., Tavor-Deslex, D., Lituiev, D., Enkerli, K., Tarr, P.T., and Müller, B. (2013). A robust and sensitive synthetic sensor to monitor the transcriptional output of the cytokinin signaling network in planta. *Plant Physiol.* 161, 1066–1075. <https://doi.org/10.1104/pp.112.211763>.
38. Arie-Bonnet, J., Carrasco, K., Le Grand, M., Hoffer, L., Betzi, S., Feracci, M., Tsvetkov, P., Devred, F., Collette, Y., Morelli, X., et al. (2020). In silico molecular target prediction unveils mebendazole as a potent MAPK14 inhibitor. *Mol. Oncol.* 14, 3083–3099. <https://doi.org/10.1002/1878-0261.12810>.
39. Mayerhofer, H., Panneerselvam, S., and Mueller-Dieckmann, J. (2012). Protein kinase domain of CTR1 from Arabidopsis thaliana promotes ethylene receptor cross talk. *J. Mol. Biol.* 415, 768–779. <https://doi.org/10.1016/j.jmb.2011.11.046>.
40. Allen, J.J., Li, M., Brinkworth, C.S., Paulson, J.L., Wang, D., Hübner, A., Chou, W.H., Davis, R.J., Burlingame, A.L., Messing, R.O., et al. (2007). A semisynthetic epitope for kinase substrates. *Nat. Methods* 4, 511–516. <https://doi.org/10.1038/nmeth1048>.
41. Fu, L., Liu, Y., Qin, G., Wu, P., Zi, H., Xu, Z., Zhao, X., Wang, Y., Li, Y., Yang, S., et al. (2021). The TOR-EIN2 axis mediates nuclear signalling to modulate plant growth. *Nature* 591, 288–292. <https://doi.org/10.1038/s41586-021-03310-y>.
42. Mou, W., Kao, Y.T., Michard, E., Simon, A.A., Li, D., Wudick, M.M., Lizzio, M.A., Feijó, J.A., and Chang, C. (2020). Ethylene-independent signaling by the ethylene precursor ACC in Arabidopsis ovular pollen tube attraction. *Nat. Commun.* 11, 4082. <https://doi.org/10.1038/s41467-020-17819-9>.
43. Li, W., Lacey, R.F., Ye, Y., Lu, J., Yeh, K.C., Xiao, Y., Li, L., Wen, C.K., Binder, B.M., and Zhao, Y. (2017). Triplin, a small molecule, reveals copper ion transport in ethylene signaling from ATX1 to RAN1. *PLoS Genet.* 13, e1006703. <https://doi.org/10.1371/journal.pgen.1006703>.
44. Qiao, H., Shen, Z., Huang, S.S.C., Schmitz, R.J., Urlich, M.A., Briggs, S.P., and Ecker, J.R. (2012). Processing and Subcellular Trafficking of ER-Tethered EIN2 Control Response to Ethylene Gas. *Science* 338, 390–393. <https://doi.org/10.1126/science.1225974>.
45. Guo, H., and Ecker, J.R. (2003). Plant responses to ethylene gas are mediated by SCF(EBF1/EBF2)-dependent proteolysis of EIN3 transcription factor. *Cell* 115, 667–677. [https://doi.org/10.1016/S0092-8674\(03\)00969-3](https://doi.org/10.1016/S0092-8674(03)00969-3).
46. Fu, L., Liu, Y., Qin, G., Wu, P., Zi, H., Xu, Z., Zhao, X., Wang, Y., Li, Y., Yang, S., et al. (2021). The TOR-EIN2 axis mediates nuclear signalling to modulate plant growth. *Nature* 591, 288–292. <https://doi.org/10.1038/s41586-021-03310-y>.
47. Furutani, M., and Morita, M.T. (2021). LAZY1-LIKE-mediated gravity signaling pathway in root gravitropic set-point angle control. *Plant Physiol.* 187, 1087–1095. <https://doi.org/10.1093/plphys/kiab219>.
48. Alonso, J.M., Stepanova, A.N., Solano, R., Wisman, E., Ferrari, S., Ausubel, F.M., and Ecker, J.R. (2003). Five components of the ethylene-response pathway identified in a screen for weak ethylene-insensitive

- mutants in *Arabidopsis*. *Proc. Natl. Acad. Sci. USA* 100, 2992–2997. <https://doi.org/10.1073/pnas.0438070100>.
49. Nakamura, M., Naoi, K., Shoji, T., and Hashimoto, T. (2004). Low concentrations of propyzamide and oryzalin alter microtubule dynamics in *Arabidopsis* epidermal cells. *Plant Cell Physiol.* 45, 1330–1334. <https://doi.org/10.1093/pcp/pch300>.
50. Liao, C.Y., Smet, W., Brunoud, G., Yoshida, S., Vernoux, T., and Weijers, D. (2015). Reporters for sensitive and quantitative measurement of auxin response (vol 12, pg 207, 2015). *Nat. Methods* 12, 1098. <https://doi.org/10.1038/nmeth1115-1098a>.
51. Schindelin, J., Arganda-Carreras, I., Frise, E., Kaynig, V., Longair, M., Pietzsch, T., Preibisch, S., Rueden, C., Saalfeld, S., Schmid, B., et al. (2012). Fiji: an open-source platform for biological-image analysis. *Nat. Methods* 9, 676–682. <https://doi.org/10.1038/nmeth.2019>.
52. Babicki, S., Arndt, D., Marcu, A., Liang, Y., Grant, J.R., Maciejewski, A., and Wishart, D.S. (2016). Heatmapper: web-enabled heat mapping for all. *Nucleic Acids Res.* 44, W147–W153. <https://doi.org/10.1093/nar/gkw419>.
53. Trott, O., and Olson, A.J. (2010). AutoDock Vina: improving the speed and accuracy of docking with a new scoring function, efficient optimization, and multithreading. *J. Comput. Chem.* 31, 455–461. <https://doi.org/10.1002/jcc.21334>.
54. Pettersen, E.F., Goddard, T.D., Huang, C.C., Couch, G.S., Greenblatt, D.M., Meng, E.C., and Ferrin, T.E. (2004). UCSF Chimera—a visualization system for exploratory research and analysis. *J. Comput. Chem.* 25, 1605–1612. <https://doi.org/10.1002/jcc.20084>.
55. Rosquete, M.R., von Wangenheim, D., Marhavý, P., Barbez, E., Stelzer, E.H.K., Benková, E., Maizel, A., and Kleine-Vehn, J. (2013). An Auxin Transport Mechanism Restricts Positive Orthogravitropism in Lateral Roots. *Curr. Biol.* 23, 817–822. <https://doi.org/10.1016/j.cub.2013.03.064>.
56. Ogura, T., Goeschl, C., and Busch, W. (2022). A Multiplexed, Time-Resolved Assay of Root Gravitropic Bending on Agar Plates. *Methods Mol. Biol.* 2368, 61–70. https://doi.org/10.1007/978-1-0716-1677-2_4.
57. Berardini, T.Z., Reiser, L., Li, D., Mezheritsky, Y., Muller, R., Strait, E., and Huala, E. (2015). The *Arabidopsis* information resource: Making and mining the "gold standard" annotated reference plant genome. *Genome* 53, 474–485. <https://doi.org/10.1002/dvg.22877>.
58. Dobin, A., Davis, C.A., Schlesinger, F., Drenkow, J., Zaleski, C., Jha, S., Batut, P., Chaisson, M., and Gingeras, T.R. (2013). STAR: ultrafast universal RNA-seq aligner. *Bioinformatics* 29, 15–21. <https://doi.org/10.1093/bioinformatics/bts635>.
59. Robinson, M.D., McCarthy, D.J., and Smyth, G.K. (2010). edgeR: a Bioconductor package for differential expression analysis of digital gene expression data. *Bioinformatics* 26, 139–140. <https://doi.org/10.1093/bioinformatics/btp616>.
60. Alexa, A., Rahnenführer, J., and Lengauer, T. (2006). Improved scoring of functional groups from gene expression data by decorrelating GO graph structure. *Bioinformatics* 22, 1600–1607. <https://doi.org/10.1093/bioinformatics/btl140>.
61. Mayerhofer, H., Mueller-Dieckmann, C., and Mueller-Dieckmann, J. (2011). Cloning, expression, purification and preliminary X-ray analysis of the protein kinase domain of constitutive triple response 1 (CTR1) from *Arabidopsis thaliana*. *Acta Crystallogr., Sect. F: Struct. Biol. Cryst. Commun.* 67, 117–120. <https://doi.org/10.1107/S1744309110047640>.

STAR★METHODS

KEY RESOURCES TABLE

REAGENT or RESOURCE	SOURCE	IDENTIFIER
Antibodies		
Recombinant Anti-Thiophosphate ester antibody	Abcam	Cat# Ab92570; RRID:AB_10562142
Chemicals, peptides, and recombinant proteins		
SP 2000 small molecule library	He et al. ³⁰	Gift from UC Riverside
Mebendazole	ACROS	Cat# 101720050
DMSO	Alfa Aesar	Cat# 36480
ACC	Sigma	Cat# A3903
IAA	Alfa Aesar	Cat# A10556
Maxima TM H Minus cDNA Synthesis Master Mix, with dsDNase	Thermo Scientific	Cat# M1682
Luna [®] Universal qPCR Master Mix	NEB	Cat# M3003L
MBP	Sigma	Cat# M1891
ATP γ S	Sigma	Cat# A1388
PNBM	CAYMANCHEMICAL	Cat# 21456-1
Deposited data		
RNA-seq of Arabidopsis root	This study	GSE201648
Experimental models: Organisms/strains		
<i>Arabidopsis: etr1-1</i>	ABRC	CS237
<i>Arabidopsis: etr1-3</i>	ABRC	CS3070
<i>Arabidopsis: ctr1-1</i>	Kieber et al. ¹⁸	N/A
<i>Arabidopsis: ein2-5</i>	Alonso et al. ¹⁹	N/A
<i>Arabidopsis: ein3-1eil1-1</i>	Alonso et al. ⁴⁸	N/A
<i>Arabidopsis: ein3 eil1 35S: EIN3-GFP</i>	He et al. ³⁰	N/A
<i>Arabidopsis: UBQ10p:TUB6-GFP</i>	Nakamura et al. ⁴⁹	N/A
<i>Arabidopsis: 35S:DR5v2:3xGFP-NLS</i>	Liao et al. ⁵⁰	Weijers lab
<i>Arabidopsis: TCSn-GFP</i>	Zürcher et al. ³⁷	Argueso lab
<i>Arabidopsis: EIN2-GFP in ein2-5</i>	Fu et al. ⁴⁶	Fu Lab
Recombinant DNA		
pET28a-CTR1-KD	This paper	N/A
pET28a-MAPK4	This paper	N/A
Commercial Kits		
Spectrum TM Plant Total RNA Kit	Sigma	Cat# STRN250
Software and algorithms		
Fiji	Schindelin et al. ⁵¹	http://fiji.sc/Fiji
GraphPad Prism	GraphPad	Version 9.3.1
Heatmapper	Babicki et al. ⁵²	http://heatmapper.ca/
AutoDock Vina	Trott and Olson ⁵³	https://vina.scripps.edu/
Chimera	Pettersen et al. ⁵⁴	https://www.cgl.ucsf.edu/chimera/

RESOURCE AVAILABILITY

Lead contact

Further information and requests for resources and reagents should be directed to and will be fulfilled by the lead contact, Wolfgang Busch (wbusch@salk.edu).

Materials availability

This study did not generate new unique reagents. The recombinant DNA of pET28a-CTR1-KD and pET28a-MAPK4 generated in this study are available from the [lead contact](#) with a completed materials transfer agreement.

Data and code availability

Data that support the findings of this study have been deposited in GEO. The GEO number is GSE201648.

- The RNA-seq data reported in this study that support the findings of this study have been deposited in GEO. The GEO number is GSE201648.
- This paper does not report original code.
- Any additional information required to reanalyze the data reported in this work paper is available from the [lead contact](#) upon request.

EXPERIMENTAL MODEL AND SUBJECT DETAILS

Arabidopsis thaliana

Arabidopsis mutants and transgenic lines used in this study are in the Col-0 background if not mentioned otherwise. *etr1-1* (CS237) and *etr1-3* (CS3070) were ordered from ABRC, *ctr1-1*¹⁸ *ein2-5*,¹⁹ *ein3-1 eil1-1*,⁴⁸ *ein3 eil1 35S: EIN3-GFP*,³⁰ and *UBQ10p:TUB6-GFP*⁴⁹ were lab stock. *35S:DR5v2:3xGFP-NLS*⁵⁰ was gift from Weijers lab (Col-Utrecht background). *TCSn-GFP*³⁷ was a gift from Argueso lab. *EIN2-GFP*⁴⁶ in *ein2-5* was a gift from Fu lab. Plants were sown on half Murashige and Skoog (MS) medium with 1% (w/v) sugar, 0.1% (w/v) MES (pH 5.75), containing 1% (w/v) agar supplemented with different chemicals as described in the article. Following a 3-day stratification in the cold room (4–10°C), for green seedling assay, plants were grown on vertical plates in a walk-in growth chamber with long day conditions (16/8 h) at 21°C, 50 μM light intensity, 60% humidity. During nighttime, temperature was decreased to 15°C. For etiolated seedling assay, the plates were placed in light for 4 h and then germinated in the dark for 3 day in the growth chamber at 22°C.

Plants were grown on vertical plates in a walk-in growth chamber with long day conditions (16/8 h) at 21°C, 50 μM light intensity, 60% humidity. During nighttime, temperature was decreased to 15°C.

Accession numbers

Sequence data from this article can be found in the Arabidopsis Genome Initiative or GenBank/EMBL databases or Uniprot databases under the following accession numbers: *ERF1* (AT3G23240), *ETR1* (AT1G66340), *CTR1* (AT5g03730), *EIN2* (AT5G03280), *EIN3* (AT3g20770), *EIL1* (AT2G27050), *MAPK4* (AT4G01370), and *hsMAPK14* (HGNC:6876). Accession numbers of protein and chemicals structures used in the molecular modeling in [Figure 6](#) are as follows: CTR1 (PDB: 3PPZ), MAPK14 (PDB: 6SFO) and MBZ (ChEMBL685).

METHOD DETAILS

Small molecule library and screen information

The SP2000 small molecule library was received from the University of California, Riverside. The library was first screened at a concentration of 50–100 μM in 200 μL of liquid MS media using wild type Arabidopsis. After being grown in the liquid media with small molecules for 7 days, seedlings were transferred to vertical plates to grow for another 2 days. The root phenotypes were acquired by CCD flatbed scanners. After candidates were picked, a second round of screen was performed by growing Col-0 seedlings on vertical plates with gradient concentration of candidate small molecules, from 1 μM to 100 μM, for 14 days to confirm the phenotype and optimal concentration.

Cloning and constructs

To produce recombinant CTR1 kinase domain (CTR1-KD) and MAPK4 proteins in *E. coli*, the coding sequences of 540–821 aa of CTR1 and full length MAPK4 were PCR amplified from cDNA of Arabidopsis Col-0, using gene-specific primers (listed in KEY RESOURCES TABLE). The PCR products were inserted into pET28a using restriction digestion and ligation with EcoR 1 and Sal 1 (NEB) sites.

Chemical solutions

The stock solutions for preparing media for the plant experiments were Mebendazole (10 mM) in DMSO, ACC (10 mM) in dH₂O, IAA (1 mM) in ethanol, DAPI (0.1 mg/mL) in PBS buffer.

Root phenotyping

Images of root phenotypes on plates were acquired with CCD flatbed scanners (EPSON). Root lengths and lateral root angles were measured using Fiji (<http://fiji.sc/Fiji>).

Lateral root angle measurement

The lateral root angle of individual LRs was measured according to⁵⁵ using Fiji. LRs after stage III from each seedling were measured according to.^{7,55}

Time lapse of lateral root angle phenotyping

14-day-old seedlings on DMSO plate or 19 d old seedling on mebendazole plate were transferred to DMSO or 1 μ M mebendazole plates as described (Figure 1E). Root phenotype images were acquired by CCD vertical scanners (EPSON) every 10 min over a period of 24 h using the tool described.⁵⁶ Root length and lateral root angles were measured using Fiji (<http://fiji.sc/Fiji>).

mRNA-seq

A. tissue preparation

Roots or lateral root tips of 14-day-old Col-0 seedlings with different treatment were collected for the mRNA-seq analysis. In detail.

A. roots

Sterilized seeds of Col-0 on $\frac{1}{2}$ MS media were planted on a mesh in one row (~more than 30 seeds/plate). 5 plates were used for one treatment condition for every replicate, and 4 replicates were used for every treatment. After 14 days of vertical growth in the chamber, liquid media of $\frac{1}{2}$ MS with DMSO (0.1%, v/v), 10 μ M MBZ, and 10 μ M ACC (to be consistent, we also added the same concentration of DMSO (0.1%, v/v) in the ACC treatment plates) were prepared. 10 mL liquid treatment medium was used on each plate. The mesh with seedlings from $\frac{1}{2}$ MS plates was transferred the respective liquid treatment plates and kept in growth chamber. After 4 h for the mRNA-seq of MBZ treatment and 3 h for the mRNA-seq of MBZ and ACC treatment, roots were collected using scalpel and tweezers. Excess liquid on the roots was removed using a paper towel. Root samples were flash-frozen in liquid nitrogen and then stored at -80°C freezer before RNA extraction.

For RNA extraction, root tissues were ground in liquid nitrogen and RNA was extracted using Quick-RNA Kits (Zymo research). RNA libraries were prepared for sequencing using standard Illumina protocols at the Salk Next Generation Sequencing Core (NGS).

Note: We used liquid media for DMSO, MBZ, and ACC treatment in the mRNA-seq of roots to detect transient gene regulation as these chemicals in liquid media can be sufficiently and equally absorbed into lateral roots and reduce time for sample collection.

B. lateral root tips

Sterilized seeds were grown for 14 days on $\frac{1}{2}$ MS medium. The seedlings were then transferred to freshly prepared DMSO or 1 μ M MBZ plates for 4 h on 15 plates (5 plants/plate) for each treatment. 4 biological replications were performed. A stereo microscope (Leica) was used to dissect the meristem area of lateral root tips in order to collect the lateral root tips. The cut lateral root tips were quickly placed into 1.5 microcentrifuge tubes that floated on liquid nitrogen. This process was repeated until approximately 400 root tips were collected per sample.

The NucleoSpin RNA extraction kit (Macherey-Nagel) was used to extract total RNA. The concentration and integrity of extracted RNA were determined using Qubit and TapeStation 2200 before being sent to Salk Next Generation Sequencing Core (NGS) for library preparation and sequencing.

B. data analysis

A. read alignment

The TAIR10 genome file and annotation file were obtained from the Arabidopsis Information resource web site (<http://www.arabidopsis.org>).⁵⁷ The An aligner, called the Splice Transcripts Alignments to Reference (STAR) version 2.7.0a,⁵⁸ was used to align short reads in the FASTQ files.

B. Differential expression analysis

Differential expression of genes between treatments and control was determined using the R package, *edgeR* (version 3.36.0).⁵⁹ The CPM (counts per million) function from *edgeR* was used to normalize the counts and differentially expressed genes (DEGs) were identified using *glmLRT* function from *edgeR*. A false discovery rate (FDR < 0.05) and $|\log_2\text{FC}| > 1$ were used as the criterial values for identification of up-regulated and down-regulated DEGs.

GO analysis

Gene Ontology analysis of up-regulated DEGs (FDR < 0.05) and $|\log_2\text{FC}| > 1$ by MBZ treatment in roots of 14-day-old Arabidopsis seedlings was performed with PANTHER Overrepresentation Test (Released 20230705). The Annotation Version used GO Ontology database (<https://doi.org/10.5281/zenodo.7942786> (Released 20230510)). Enriched genes (Bonferroni-corrected for $p < 0.05$) for biological processes were listed (Figure 2A).

We used R package topGO (version 2.42.0)⁶⁰ with the weight01 algorithm and the mappings from the “org.At.tair.db” R package to perform functional enrichment analysis of DEGs by MBZ treatment in roots and lateral root tips of 14-day-old Arabidopsis seedlings. We carried out KS test for statistical comparison. Then we used “ggplot2” package in R to plot 30 most enriched gene ontology terms (GO) which were ordered by Kolmogorov-Smirnov p values for biological processes (Figures 2F and S2D).

Measurement of ethylene production

100 seeds of Col-0 were planted and sealed in a screw-top 20 mL vial containing 10 mL $\frac{1}{2}$ MS medium supplemented with DMSO (control), 10 μ M mebendazole, and 10 μ M ACC treatments (4 replicates). These vials were incubated at 22°C for 3 days under dark environment. 500–1000 μ L sample of the headspace gas was sampled with an autosampler (TriPlus RSH, Thermo Scientific) and injected into a gas chromatograph (Trace 1310 GC, Thermo Scientific) that was equipped with an HP-PLOTQ column (30 mm, 320 μ m, 20 μ m) and a mass spectrometer (TSQ8000 Evo MS, Thermo Scientific), scanning from 25–27.5 m/z. Separations were carried out at 35°C using He as the carrier gas. The area of the ethylene peak (RT: 4 min) was integrated using Thermo Xcalibur Qual Browser. A calibration curve was generated by varying the injection volume (100 μ L, 250 μ L, 500 μ L, and 1000 μ L) of a 10 ppm ethylene standard (in nitrogen), and sample results are expressed as concentrations calculated from linear regression of calibration samples.

Microscopy

A Zeiss 710 confocal microscope with a 40x objective was used to detect propidium iodide (PI) fluorescence in Figure 3F. A Keyence BZ-X810 microscope with a 20x objective was used to detect bright field images and GFP fluorescence in Figures 3B and S1B right panel. A Leica TCS SP5 confocal microscope with 40x objective was used to detect GFP fluorescence in Figure 7A. An Olympus FLUOVIEW FV3000 confocal microscope with 40x objective was used to detect GFP fluorescence and DAPI-stained nuclei in Figure S5.

Accumulation of EIN2-GFP in root cells

3-day-old etiolated seedlings of two independent transgenic *EIN2-GFP* reporter lines in which the GFP was fused to EIN2's C terminus (*pEIN2::EIN2-GFP* in the *ein2-5* background⁴¹) were moved into different wells of 6-well plate with 5 mL Mock (dH₂O + 5 μ L DMSO), ACC (100 μ M + 5 μ L DMSO), or MBZ (10 μ M). The plate was then covered with tin foil to keep the dark environment for 3 h. Then samples were directly mounted on glass slides in their treatment liquid and observed under a Leica SP5 microscope (Leica). DAPI staining used 0.5 μ g/mL DAPI solution for 30 min and was observed under an Olympus FLUOVIEW FV3000 microscope (Olympus).

Time lapse microscopy of reporter genes in lateral root tips

To observe the response of ethylene (*EIN3-GFP*), auxin (*DR5v2-GFP*), and cytokinin (*TCSn-GFP*) reporter lines to MBZ, 14-day-old seedlings grown on $\frac{1}{2}$ MS media were transferred to a Chambered Coverglass (Thermo Scientific) that was filled with treatment medium. For chamber preparation, 6 mL of $\frac{1}{2}$ MS medium (1% agar) supplemented with the different treatments (DMSO, 10 μ M MBZ, 1 μ M IAA, 50 μ M ACC, and 10 μ M tZ) was filled to each chamber. After 20 min of medium solidification, the seedlings were placed on the media surface and the lateral roots were adjusted to positions suitable for imaging.

For imaging, a Zeiss CSU Spinning Disk Confocal Microscope equipped with laser 488 nm and a Yokogawa spinning disk scan head with EM-CCD camera were used to set up the image acquisition every 20 min for a total of 4 h. Three z stack positions were automatically captured at each time point under 10X objective and Fiji was used to quantify the average intensity of GFP fluorescence. For proper comparison at different treatment conditions of each reporter lines, we normalized the average fluorescence data as the percentages (or relative fluorescence intensity as text label). In detail, the first time point of each treatment is set as 100% and the relative fluorescence intensity from the second time point is calculated as the fold-change in percentages comparing the first time point.

Quantification of relative GFP fluorescent intensity between the nucleus and cytosol

The quantification of the microscopy localization data of *EIN2-GFP* in Figure 7B was done according to⁴¹ using LAS X (Leica Application Suite v. X3.1.1.15751) and GraphPad Prism V9.5.1. In brief, the signal intensity of nucleus (Ni) and whole cell (Wi) was quantified by LAS X (Mean value of nucleus * ROI Area of nucleus, mean value of whole cell * ROI Area of whole cell), and then the signal intensity of cytosol (Ci) was obtained by Wi minus Ni, and the area of cytosol (Sc) was obtained by the area of whole cell (ROI Area of whole cell) minus the area of nucleus (ROI Area of nucleus). The mean value of the signal intensity of cytosol (Mean Ci) equals Ci/Sc, and the relative GFP fluorescent intensity between the nucleus and cytosol equals Mean value of nucleus/Mean Ci.

Computational docking and molecular modeling

The AutoDock Vina and Chimera software were used to dock mebendazole (ChEMBL685) into crystal structure of CTR1 (PDB: 3PPZ) and MAPK14 (PDB: 6SFO). Figures for those structures were visualized and generated by Chimera and Pymol.

Protein purification

The CTR1 Kinase domain (540 aa–821 aa) (CTR1-KD) and MAPK4 were cloned into a pET28a. Proteins were expressed in Rosetta 2(DE3)pLysS Competent Cells. Cultures were incubated at 37°C (OD 600:0.7 to 0.9) and induced by adding 0.4 mM isopropylthio- β -D-galactoside (IPTG) at 20°C for 22 h, 200 rpm. Cells were harvested and resuspended in lysis buffer (50 mM pH 7.5 Tris-HCl, 1 mM EDTA, 100 mM NaCl, 20% glycerol, EDTA-free protease inhibitor cocktail, 10 mM imidazole). followed by sonication and centrifugation (13,000 \times g \times 20 min). The His-tagged proteins were first purified using QIAGEN Ni-NTA Agarose. The elute from Ni-NTA was

collected and further purified by FPLC using superdex 200 Increase 10/300 column.⁶¹ The fractions corresponding to single peak from FPLC were combined, and concentrated to a desired volume. Protein purity was verified by Coomassie blue gel staining. Protein concentration was measured by their absorbance at 280 nm.

***In vitro* kinase assay with non-radioactive ATP- γ -S**

The *in vitro* kinase assay followed the previous published method.⁴⁰ 100 ng purified recombinant CTR1-KD or 1 μ g MPK4 was mixed with 2 μ g Myelin Basic Protein (MBP, a common kinase substrate, Sigma Cat. M1891) and 1 mM ATP γ S in kinase reaction buffer (10 mM HEPES pH 7.4, 150 mM NaCl, 10 mM MgCl₂, 1xRoche Complete Protease Inhibitor mixture) and different concentration of MBZ at room temperature and vortexed for 1 h. The reactions were terminated by 20 mM EDTA, and the proteins were alkylated by 1.5 μ L of 50 mM PNBM (CAYMAN CHEMICAL CO, Cat. 21456-1) at room temperature and vortexed for 2 h. This step was terminated by denaturing in NuPAGE LDS Sample Buffer and 1x NuPAGE Sample Reducing Agent (Invitrogen). Samples were subjected to SDS-PAGE. The phosphorylation status of MBP, CTR1-KD and MPK4 were analyzed by western blot using Recombinant Anti-Thiophosphate ester antibody (Abcam, Cat. Ab92570, 1:5000).

QUANTIFICATION AND STATISTICAL ANALYSIS

A two-sided Student's t-test was used for comparisons of two conditions. The comparison of meristem length, mature cell length, root length, GSA between multiple treatments or genotypes was performed by One-way ANOVA and *post hoc* Tukey testing. Detailed information was prepared in figure legends. Statistical significance of overlap between DEGs from MBZ treatment and ethylene treatment was assessed by hypergeometric distribution test.

Supplemental information

Identification of mebendazole as an ethylene signaling activator reveals a role of ethylene signaling in the regulation of lateral root angles

Wenrong He (何文容), Hai An Truong, Ling Zhang (张凌), Min Cao (曹珉), Neal Arakawa, Yao Xiao (肖瑶), Kaizhen Zhong (钟开珍), Yingnan Hou (侯英楠), and Wolfgang Busch

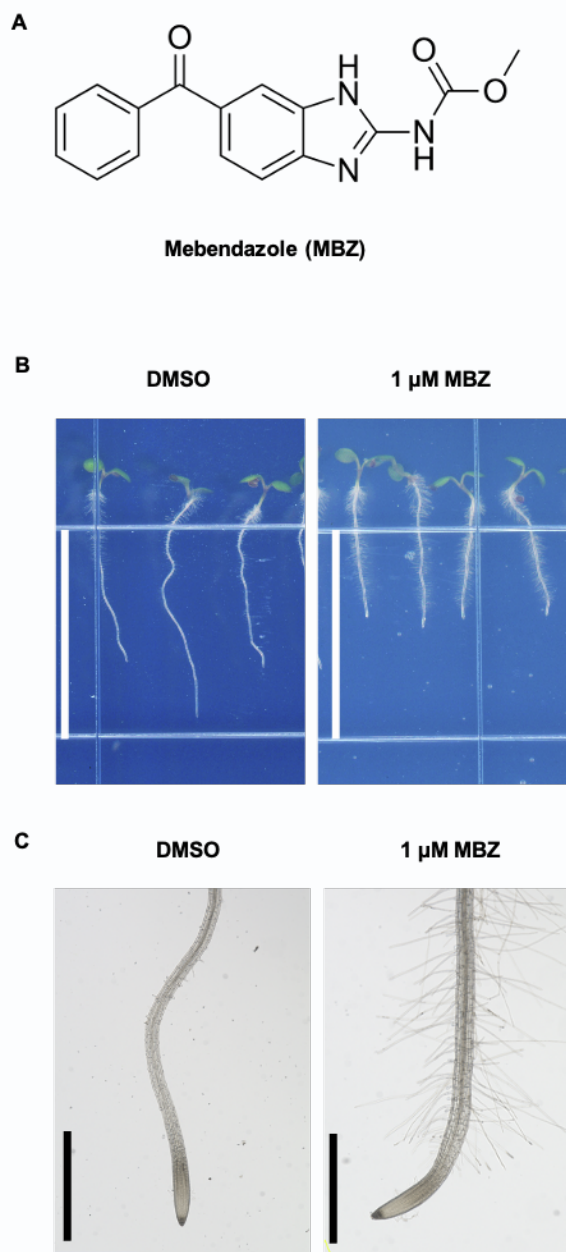


Figure S1. MBZ treatment affects root growth and development
 (A) Chemical structure of MBZ.

(B-C) Root hair phenotype of 7-day-old seedlings on DMSO and 1 μ M MBZ plates recorded by a scanner (B) or a microscope (C). 20 seedlings were observed on left panel and 10 seedlings were observed on right panel. (Scale bar: **B**, 13 mm; **C**, 1000 μ m)

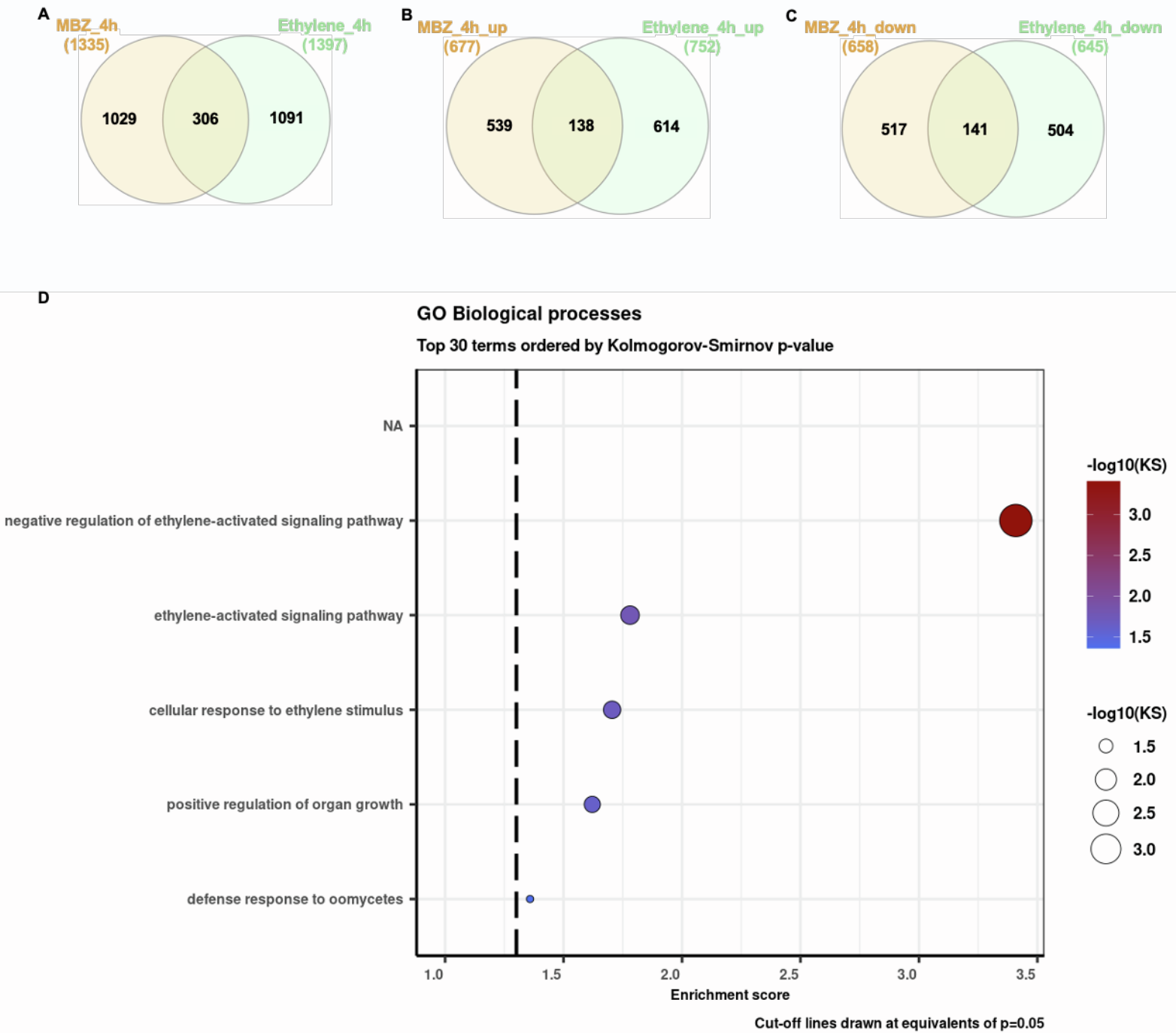


Figure S2. The analysis of differentially expressed genes (DEGs) by MBZ treatment.

(A-C) Venn diagrams showing differentially expressed genes in 4 h MBZ treatment in roots of 14-day-old green seedlings and published 4 h ethylene treatment in 3-day-old etiolated seedlings. All genes ($FDR < 0.05$; $abs(\log_2)$ fold change > 1) (A), upregulated genes ($FDR < 0.05$; \log_2 fold change > 1) (B), downregulated genes ($FDR < 0.05$; \log_2 fold change < -1) (C).

(D) Gene ontology (GO) analysis of upregulated genes ($FDR < 0.05$; \log_2 fold change > 1) from DEGs upon MBZ treatment.

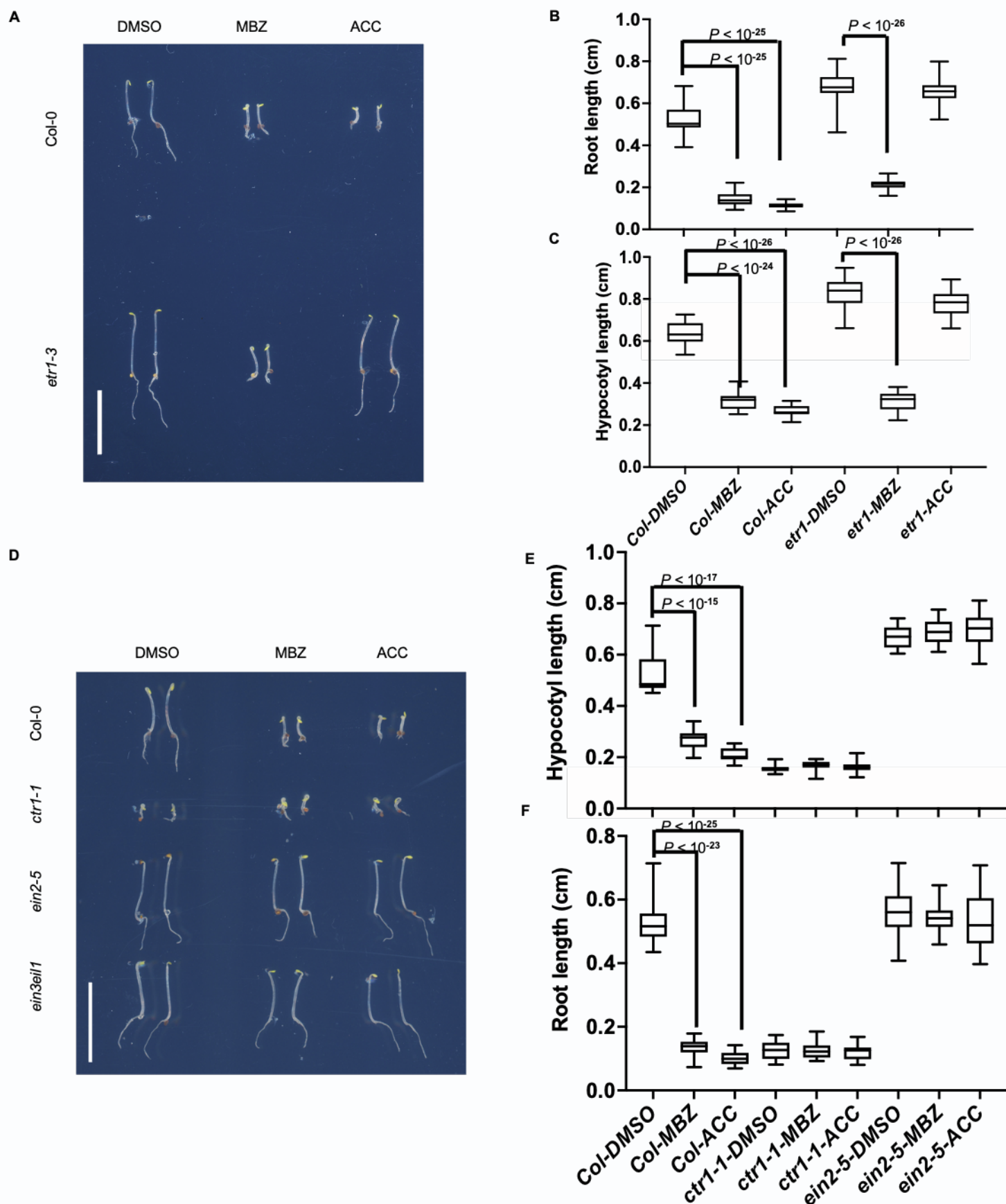


Figure S3. Etiolated seedling phenotypes in mutants of the ethylene pathway.

(A) 4-day-old etiolated seedlings of Col-0 and *etr1-3* grown on DMSO, 2.5 μ M MBZ, and 10 μ M ACC plates.

(B-C) Quantification of hypocotyl length (B) and root length (C) of seedlings in (A). 20 seedlings were quantified.

(D) 4-day-old etiolated seedlings of Col-0, *ctr1-1*, *ein2-5*, and *ein3eil1* grown on DMSO, 2.5 μ M MBZ, and 10 μ M ACC plates.

(E-F) Quantification of hypocotyl length (E) and root length (F) of seedlings in D. 20 seedlings were quantified. Statistical analysis in B, C and E, F were done using unpaired, two-tailed Student's t-tests. P-values are indicated in the figure. (Scale bar: A, D, 1 cm). Whiskers: min/max values; hinges: 25th to 75th percentile; mid-line: median.

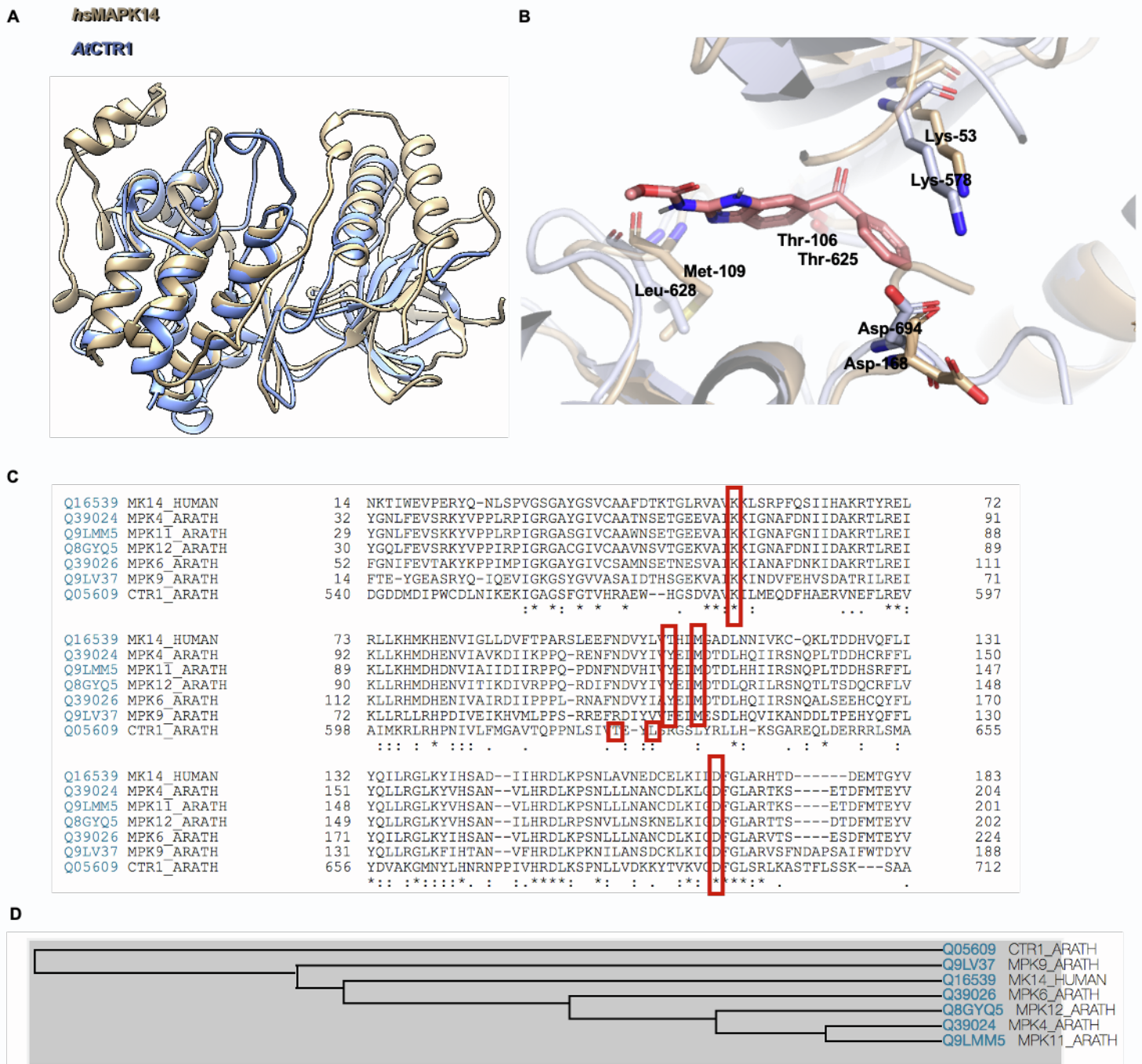


Figure S4. Alignment of AtCTR1-KD and *hsMAPK14*

- (A) The structure alignment of *hsMAPK14* (coppery) and CTR1-KD (celeste).
 (B) The protein binding sites in *hsMAPK14* (coppery) and CTR1-KD (periwinkle) with highlighted key residues.
 (C) Sequence alignment of kinase domains. Key residues in MAPK14_human and CTR1-KD in Arabidopsis are indicated by red boxes.
 (D) Phylogenetic analysis of kinases aligned in (C).

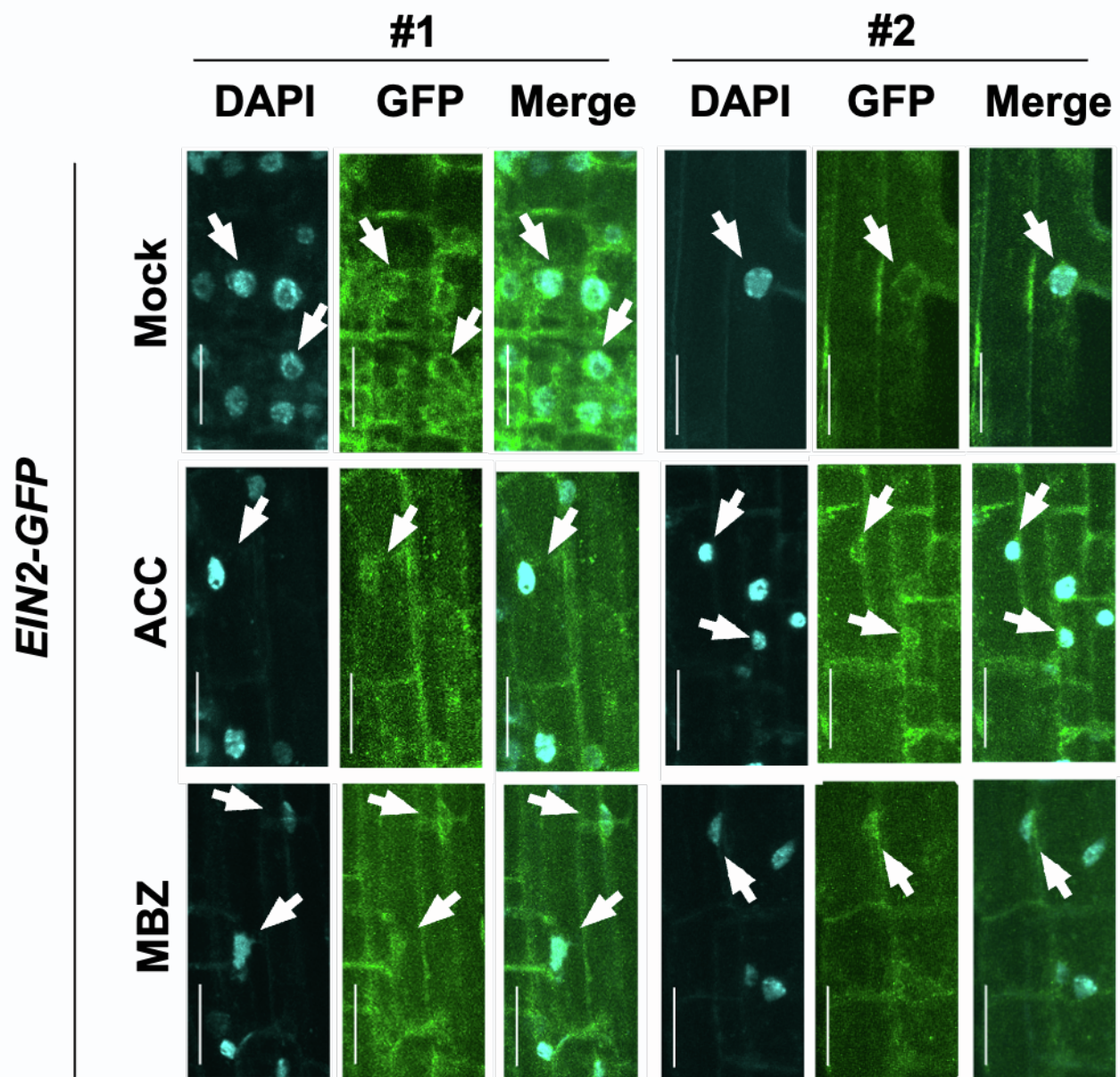


Figure S5. DAPI staining of *EIN2-GFP* reporter lines.

DAPI staining of nuclear localization of *EIN2-GFP* in root cells. 3-day-old etiolated seedlings treated with Mock, ACC (100 μ M), or MBZ (10 μ M) for 3 hours. Arrows indicate nuclei. (Scale bar: 20 μ m). While in mock treatment there is no signal visible within nuclei, upon ACC and MBZ treatments signal is visible in nuclei.

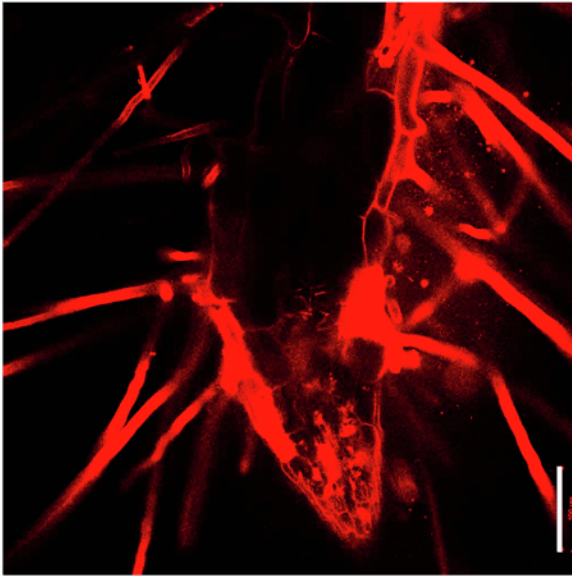
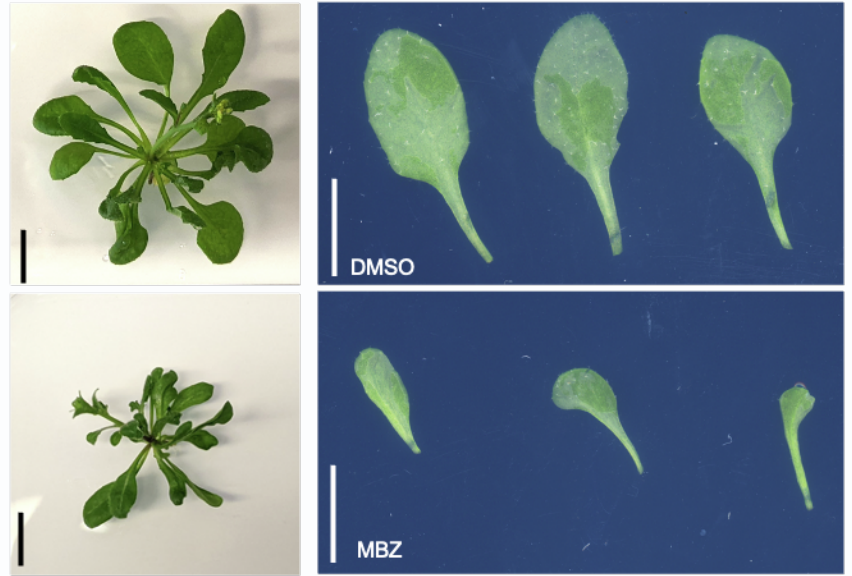
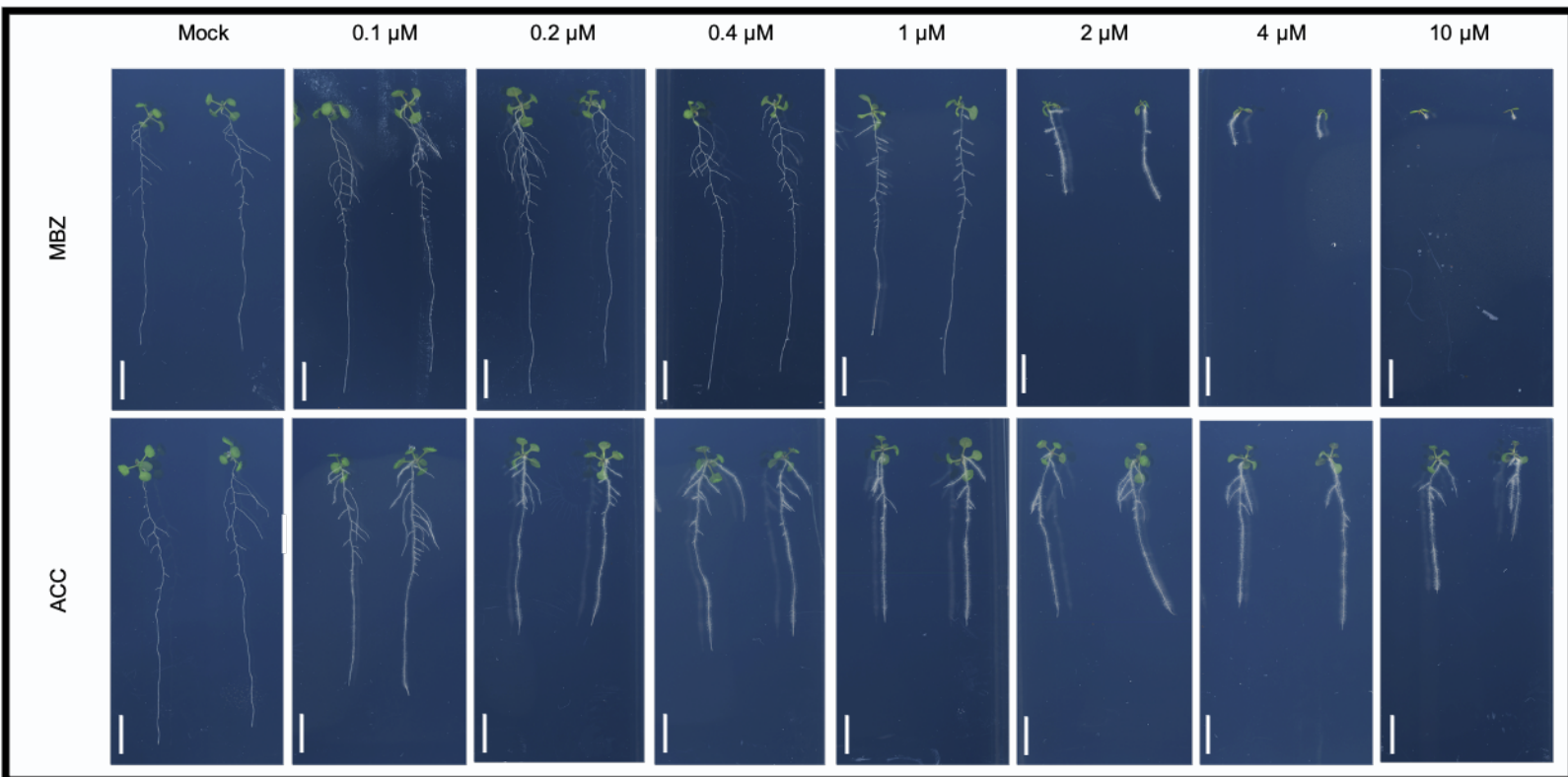
A**B****C**

Figure S6. High concentrations or long-term treatment of MBZ induce phenotypes that go beyond ethylene induced effects

(A) Confocal microscopy images of a root meristem of 4-day-old etiolated WT seedling grown on 10 μ M MBZ plate.

(B) 38-day-old Col-0 plants grown on DMSO and 1.2 μ M MBZ plates.

(C) 14-day-old seedlings of Col-0 grown on increasing concentrations MBZ and ACC (0.1, 0.2, 0.4, 1, 2, 4, 10 μ M) 20 seedlings were observed.

Similar results were obtained from three biological replicates of the experiment. (Scale bar: **A**, 100 μ m, **B**, **C**, 1 cm)

Table S1. The list of blast hits in Arabidopsis using the MAPK14_human sequence as BLASTP.

Description	Scientific Name	Max Score	Total Score	Query Cover	E value	Per. Ident	Acc. Len	Accession
MAP kinase 4 [Arabidopsis thaliana]	Arabidopsis thaliana	346	346	93%	3E-117	51.18	376	NP_192046.1
mitogen-activated protein kinase 4 [Arabidopsis thaliana]	Arabidopsis thaliana	346	346	93%	3E-117	51.18	376	ABR46146.1
mitogen-activated protein kinase 4 [Arabidopsis thaliana]	Arabidopsis thaliana	345	345	93%	8E-117	50.88	376	ABR46148.1
MAP kinase [Arabidopsis thaliana]	Arabidopsis thaliana	345	345	93%	9E-117	50.88	376	BA04867.1
mitogen-activated protein kinase 4 [Arabidopsis thaliana]	Arabidopsis thaliana	344	344	93%	1E-116	50.88	376	ABR46162.1
unnamed protein product [Arabidopsis thaliana]	Arabidopsis thaliana	340	340	95%	8E-115	47.71	376	VYS82299.1
MPK5 [Arabidopsis thaliana]	Arabidopsis thaliana	339	339	95%	9E-115	47.71	376	OAO98154.1
MAP kinase 11 [Arabidopsis thaliana]	Arabidopsis thaliana	337	337	93%	6E-114	49.71	369	NP_001117210.1
unnamed protein product [Arabidopsis thaliana]	Arabidopsis thaliana	337	337	93%	6E-114	49.71	369	CA0154293.1
MAP kinase 5 [Arabidopsis thaliana]	Arabidopsis thaliana	337	337	95%	8E-114	47.43	376	NP_567378.4
unnamed protein product [Arabidopsis thaliana]	Arabidopsis thaliana	336	336	95%	2E-113	46.84	370	CAD5324945.1
MAP kinase [Arabidopsis thaliana]	Arabidopsis thaliana	335	335	95%	2E-113	46.55	370	BA04866.1
mitogen-activated protein kinase 3 [Arabidopsis thaliana]	Arabidopsis thaliana	335	335	95%	2E-113	46.55	370	NP_190150.1
MAP kinase [Arabidopsis thaliana]	Arabidopsis thaliana	330	330	95%	3E-111	46.57	376	BA04868.1
mitogen-activated protein kinase 12 [Arabidopsis thaliana]	Arabidopsis thaliana	329	329	92%	9E-111	49.26	372	NP_182131.2
mitogen-activated protein kinase 12 [Arabidopsis thaliana]	Arabidopsis thaliana	330	330	92%	2E-110	49.26	406	NP_001325006.1
mitogen-activated protein kinase 6 [Arabidopsis thaliana]	Arabidopsis thaliana	323	323	95%	2E-108	46.84	364	6DTL_A
Crystal structure of Arabidopsis thaliana MPK6 [Arabidopsis thaliana]	Arabidopsis thaliana	323	323	95%	3E-108	46.84	370	5C06_A
unnamed protein product [Arabidopsis thaliana]	Arabidopsis thaliana	323	323	92%	3E-108	46.31	393	VYS60924.1
MAP kinase 6 [Arabidopsis thaliana]	Arabidopsis thaliana	323	323	95%	4E-108	46.84	395	NP_181907.1
MAP kinase 10 [Arabidopsis thaliana]	Arabidopsis thaliana	323	323	92%	4E-108	46.31	393	NP_191538.1
unnamed protein product [Arabidopsis thaliana]	Arabidopsis thaliana	323	323	92%	5E-108	46.31	393	CA0387508.1
MPK10 [Arabidopsis thaliana]	Arabidopsis thaliana	323	323	92%	6E-108	46.31	393	OAP05435.1
unnamed protein product [Arabidopsis thaliana]	Arabidopsis thaliana	321	321	92%	2E-107	46.02	393	CAD5326291.1
MAP kinase [Arabidopsis thaliana]	Arabidopsis thaliana	318	318	95%	2E-106	46.29	373	CAB51417.1
Protein kinase superfamily protein [Arabidopsis thaliana]	Arabidopsis thaliana	317	317	92%	4E-106	47.79	363	NP_001030990.1
unnamed protein product [Arabidopsis thaliana]	Arabidopsis thaliana	316	316	92%	8E-106	47.79	363	CAD5312051.1
mitogen-activated protein kinase homolog 2 [Arabidopsis thaliana]	Arabidopsis thaliana	316	316	85%	2E-105	49.68	376	NP_564746.1
ATMPK1 [Arabidopsis thaliana]	Arabidopsis thaliana	315	315	93%	2E-105	46.33	370	BA03535.1
unnamed protein product [Arabidopsis thaliana]	Arabidopsis thaliana	315	315	93%	3E-105	46.33	370	CA0186271.1
ATTG10210 [Arabidopsis thaliana]	Arabidopsis thaliana	315	315	93%	3E-105	46.33	370	BAH19911.1
mitogen-activated protein kinase 1 [Arabidopsis thaliana]	Arabidopsis thaliana	315	315	93%	3E-105	46.33	370	NP_001031017.1
mitogen-activated protein kinase 14 [Arabidopsis thaliana]	Arabidopsis thaliana	315	315	95%	3E-105	45.04	361	NP_195363.1
ATMPK2 [Arabidopsis thaliana]	Arabidopsis thaliana	315	315	85%	4E-105	49.35	376	BA03536.1
unnamed protein product [Arabidopsis thaliana]	Arabidopsis thaliana	313	313	95%	1E-104	45.04	361	CA0397686.1
MPK14 [Arabidopsis thaliana]	Arabidopsis thaliana	311	311	95%	8E-104	44.76	361	OAO98488.1
MAP kinase 5-CT [Arabidopsis thaliana]	Arabidopsis thaliana	310	310	81%	9E-104	50	337	ADZ76491.1
MAP kinase 7 [Arabidopsis thaliana]	Arabidopsis thaliana	310	310	85%	2E-103	48.71	368	NP_179409.1
MPK7 [Arabidopsis thaliana]	Arabidopsis thaliana	310	310	85%	2E-103	48.71	368	OAP11028.1
MAP kinase [Arabidopsis thaliana]	Arabidopsis thaliana	309	309	86%	4E-103	50.48	354	AAB61033.1
unnamed protein product [Arabidopsis thaliana]	Arabidopsis thaliana	310	310	91%	4E-103	48.49	389	CAD5321516.1
unnamed protein product [Arabidopsis thaliana]	Arabidopsis thaliana	309	309	85%	5E-103	48.71	368	CA0364931.1
MAP kinase 11 [Arabidopsis thaliana]	Arabidopsis thaliana	307	307	78%	2E-102	52.08	346	NP_001322112.1
MAP kinase [Arabidopsis thaliana]	Arabidopsis thaliana	306	306	85%	1E-101	48.06	368	BA04870.1
unnamed protein product [Arabidopsis thaliana]	Arabidopsis thaliana	310	310	86%	3E-99	48.12	716	CAD5330118.1
mitogen-activated protein kinase 12 [Arabidopsis thaliana]	Arabidopsis thaliana	297	297	80%	5E-99	51.03	324	NP_001189755.1
mitogen-activated protein kinase 16 [Arabidopsis thaliana]	Arabidopsis thaliana	287	287	91%	7E-92	42.77	567	NP_197402.1
Unknown protein [Arabidopsis thaliana]	Arabidopsis thaliana	287	287	91%	7E-92	42.77	567	AAL32607.1
unnamed protein product [Arabidopsis thaliana]	Arabidopsis thaliana	287	287	91%	9E-92	42.77	569	CAD5332107.1
MAP kinase [Arabidopsis thaliana]	Arabidopsis thaliana	276	276	75%	6E-90	50	360	BA095376.10
putative MAP kinase [Arabidopsis thaliana]	Arabidopsis thaliana	271	271	90%	4E-87	42.6	431	AAK62464.1
MPK15 [Arabidopsis thaliana]	Arabidopsis thaliana	274	274	92%	1E-86	41.86	575	OAP17567.1
MAP kinase 19 [Arabidopsis thaliana]	Arabidopsis thaliana	268	268	91%	3E-86	42.18	425	NP_001326968.1
MAP kinase 15 [Arabidopsis thaliana]	Arabidopsis thaliana	272	272	92%	4E-86	41.86	576	NP_565070.2
MPK6 [Arabidopsis thaliana]	Arabidopsis thaliana	269	269	92%	1E-84	42.15	588	OAP18797.1
unnamed protein product [Arabidopsis thaliana]	Arabidopsis thaliana	268	268	92%	1E-84	42.15	581	CAD5313053.1
mitogen-activated protein kinase [Arabidopsis thaliana]	Arabidopsis thaliana	269	269	91%	1E-84	42.18	593	BAB02403.1
unnamed protein product [Arabidopsis thaliana]	Arabidopsis thaliana	269	269	92%	2E-84	42.15	588	CA0216876.1
Protein kinase superfamily protein [Arabidopsis thaliana]	Arabidopsis thaliana	269	269	92%	2E-84	42.15	589	NP_001185027.1
MAP kinase 19 [Arabidopsis thaliana]	Arabidopsis thaliana	269	269	91%	2E-84	42.18	598	NP_188090.2
unnamed protein product [Arabidopsis thaliana]	Arabidopsis thaliana	268	268	91%	2E-84	42.18	586	VYS67392.1
unnamed protein product [Arabidopsis thaliana]	Arabidopsis thaliana	269	269	91%	2E-84	42.18	598	CA0382447.1
MAP kinase 9 [Arabidopsis thaliana]	Arabidopsis thaliana	265	265	91%	3E-84	41.3	505	NP_001327297.1
MAP kinase 9 [Arabidopsis thaliana]	Arabidopsis thaliana	266	266	91%	3E-84	41.3	510	NP_566595.1
ATMPK9 [Arabidopsis thaliana]	Arabidopsis thaliana	265	265	92%	1E-83	41.86	543	BA082222.1
unnamed protein product [Arabidopsis thaliana]	Arabidopsis thaliana	265	265	91%	2E-83	41.3	565	CAD5323398.1
unnamed protein product [Arabidopsis thaliana]	Arabidopsis thaliana	266	266	91%	5E-83	41.3	626	CA0382817.1
At4g1330 [Arabidopsis thaliana]	Arabidopsis thaliana	254	254	67%	5E-83	50.4	250	ABK59683.1
MAP kinase 9 [Arabidopsis thaliana]	Arabidopsis thaliana	265	265	91%	5E-83	41.3	619	NP_001327298.1
unnamed protein product [Arabidopsis thaliana]	Arabidopsis thaliana	265	265	91%	6E-83	41.3	620	VYS67757.1
MPK9 [Arabidopsis thaliana]	Arabidopsis thaliana	265	265	91%	7E-83	41.3	620	OAP04882.1
MAP kinase 20 [Arabidopsis thaliana]	Arabidopsis thaliana	261	261	91%	9E-83	41	468	NP_001324574.1
MAP kinase 9 [Arabidopsis thaliana]	Arabidopsis thaliana	265	265	91%	1E-82	41.3	648	NP_001327296.1
MAP kinase 17 [Arabidopsis thaliana]	Arabidopsis thaliana	261	261	91%	1E-82	40.41	486	NP_001030939.1
MAP kinase 11 [Arabidopsis thaliana]	Arabidopsis thaliana	254	254	61%	2E-82	54.46	275	NP_001322113.1
MPK20 [Arabidopsis thaliana]	Arabidopsis thaliana	261	261	91%	9E-82	41	593	OAP09267.1
MPK20 [Arabidopsis thaliana]	Arabidopsis thaliana	261	261	91%	1E-81	41	594	OAP09266.1
mitogen-activated protein kinase 18 [Arabidopsis thaliana]	Arabidopsis thaliana	262	262	91%	1E-81	41	615	NP_175756.2
MAP kinase 20 [Arabidopsis thaliana]	Arabidopsis thaliana	261	261	91%	1E-81	41	606	NP_565989.1
Contains similarity to ATMPK9 from Arabidopsis thaliana gh A03066	Arabidopsis thaliana	261	261	91%	1E-81	41	603	AAF78438.1
unnamed protein product [Arabidopsis thaliana]	Arabidopsis thaliana	261	261	91%	2E-81	39.84	623	CAD5323082.1
ATMPK9 [Arabidopsis thaliana]	Arabidopsis thaliana	258	258	91%	2E-81	40.71	510	BA082223.1
putative MAP kinase [Arabidopsis thaliana]	Arabidopsis thaliana	257	257	89%	1E-80	40.84	516	AK067338.1
Protein kinase superfamily protein [Arabidopsis thaliana]	Arabidopsis thaliana	248	248	60%	2E-80	54.02	254	NP_172266.2
MPK19 [Arabidopsis thaliana]	Arabidopsis thaliana	257	257	91%	1E-79	38.89	637	OAP01391.1
T10022.12 [Arabidopsis thaliana]	Arabidopsis thaliana	248	248	92%	1E-76	39.72	588	AAF78388.1
unnamed protein product [Arabidopsis thaliana]	Arabidopsis thaliana	241	241	91%	3E-75	38.94	471	CAD5317842.1
MAP kinase 9 [Arabidopsis thaliana]	Arabidopsis thaliana	217	217	71%	2E-66	42.7	422	NP_974331.1
hypothetical protein AXK17_AT2G00430 [Arabidopsis thaliana]	Arabidopsis thaliana	205	205	63%	9E-64	44.3	258	OAP10058.1
unnamed protein product [Arabidopsis thaliana]	Arabidopsis thaliana	212	212	91%	7E-63	36.28	581	CAD5315439.1
cell division control 2 [Arabidopsis thaliana]	Arabidopsis thaliana	185	185	79%	2E-55	38.1	294	NP_566911.1
unnamed protein product [Arabidopsis thaliana]	Arabidopsis thaliana	184	184	79%	3E-55	38.23	293	VYS59782.1
CELL DIVISION CONTROL PROTEIN 2 HOMOLOG A [Arabidopsis thaliana]	Arabidopsis thaliana	182	182	79%	2E-54	37.76	294	CAB87903.1
kinase-like protein [Arabidopsis thaliana]	Arabidopsis thaliana	181	181	79%	4E-54	36.43	290	CA016700.1
Protein kinase superfamily protein [Arabidopsis thaliana]	Arabidopsis thaliana	186	186	79%	7E-54	38	478	NP_001119484.1
AT3g48750/T21J18_20 [Arabidopsis thaliana]	Arabidopsis thaliana	180	180	78%	2E-53	37.8	297	AAL91258.1
Protein kinase superfamily protein [Arabidopsis thaliana]	Arabidopsis thaliana	182	182	79%	1E-52	36.3	461	NP_567574.1
Protein kinase superfamily protein [Arabidopsis thaliana]	Arabidopsis thaliana	185	185	79%	1E-52	38	612	NP_001190605.1
hypothetical protein AXK17_AT4G22570 [Arabidopsis thaliana]	Arabidopsis thaliana	182	182	79%	1E-52	36.3	461	OAO97644.1
CDK1 [Arabidopsis thaliana]	Arabidopsis thaliana	185	185	79%	1E-52	38	612	OAO92015.1